

Study of long-range orders of hard-core bosons coupled to cooperative normal modes in two-dimensional lattices

A. Ghosh and S. Yarlagadda

CMP Division, Saha Institute of Nuclear Physics, HBNI, Kolkata, India

(Received 22 May 2017; revised manuscript received 18 August 2017; published 6 September 2017)

Understanding the microscopic mechanism of coexisting long-range orders (such as lattice supersolidity) in strongly correlated systems is a subject of immense interest. We study the possible manifestations of long-range orders, including lattice-supersolid phases with differently broken symmetry, in a two-dimensional square lattice system of hard-core bosons (HCBs) coupled to archetypal cooperative/coherent normal-mode distortions such as those in perovskites. At strong HCB-phonon coupling, using a duality transformation to map the strong-coupling problem to a weak-coupling one, we obtain an effective Hamiltonian involving nearest-neighbor, next-nearest-neighbor, and next-to-next-nearest-neighbor hoppings and repulsions. Using stochastic series expansion quantum Monte Carlo, we construct the phase diagram of the system. As coupling strength is increased, we find that the system undergoes a first-order quantum phase transition from a superfluid to a checkerboard solid at half-filling and from a superfluid to a diagonal striped solid [with crystalline ordering wave vector $\vec{Q} = (2\pi/3, 2\pi/3)$ or $(2\pi/3, 4\pi/3)$] at one-third filling without showing any evidence of supersolidity. On tuning the system away from these commensurate fillings, checkerboard supersolid is generated near half-filling whereas a rare diagonal striped supersolid is realized near one-third filling. Interestingly, there is an asymmetry in the extent of supersolidity about one-third filling. Within our framework, we also provide an explanation for the observed checkerboard and stripe formations in $\text{La}_{2-x}\text{Sr}_x\text{NiO}_4$ at $x = 1/2$ and $x = 1/3$.

DOI: [10.1103/PhysRevB.96.125108](https://doi.org/10.1103/PhysRevB.96.125108)

I. INTRODUCTION

The origin and character of lattice supersolidity [1] [i.e., the single-phase coexistence of superconductivity/superfluidity and charge density wave (CDW) realized in discrete lattices] in naturally formed and artificially designed systems is a central issue in condensed matter physics. While phenomenological pictures [2,3] exist to explain lattice-supersolidity, a microscopic theory that elucidates the homogeneous coexistence is yet to be formulated. Supersolidity is observed in a variety of lattice systems such as the three-dimensional doped BaBiO_3 [3,4], the layered dichalcogenides [5], and molecular crystals [6], and the quasi-one-dimensional doped trichalcogenide NbSe_3 [7], and doped spin ladder $\text{Sr}_{14}\text{Cu}_{24}\text{O}_{41}$ [8,9]. Of importance are the class of materials that display superconductivity and diagonal long-range order due to strong electron-phonon interaction such as K or Pb doped BaBiO_3 (where a 10% change in the Bi–O bond length [10] has been observed) and the alkali metal fullerenes [11]. Interestingly, BaBiO_3 assumes perovskite structure with two adjacent oxygen octahedra sharing an oxygen leading to a cooperative breathing mode (CBM). Furthermore, BaBiO_3 displays valence disproportionation with local Cooper pairs [i.e., hard-core bosons (HCBs)] being formed and these HCBs couple to the CBM [12].

As regards artificially engineered systems, cold bosonic atoms in optical lattices provide a fertile playground for actualizing exotic phases such as lattice-supersolid phases with differently broken symmetry. In fact, only recently supersolidity was experimentally produced in an optical lattice by generating effective long-range interactions using a vacuum mode of an optical cavity [13]. On the theoretical side, lattice supersolidity has been realized in two-dimensional (2D) square [14–23], triangular [24–30], and honeycomb [31,32] lattices as well as in a one-dimensional lattice [33–35]. By using extended

boson Hubbard models involving hard-core bosons, commensurate supersolid has been unobtainable in unfrustrated systems such as square lattices. On the other hand, supersolids can be realized in square lattices at incommensurate fillings by a mechanism where particles (i.e., interstitials) or holes (i.e., vacancies) doped into a perfect crystal form a condensate by delocalizing in the crystalline order. Furthermore, although striped supersolidity has been achieved in Refs. [16,18] on square lattices, it is nondiagonal and characterized by density ordering wave vector $(\pi, 0)$ or $(0, \pi)$. Even though diagonal stripes [characterized by crystalline ordering wave vector $(2\pi/3, 2\pi/3)$ or $(2\pi/3, 4\pi/3)$] have been observed in systems such as $\text{La}_{2-x}\text{Sr}_x\text{NiO}_4$ (LSNO) at $x = 1/3$ hole doping [36–42] and predicted theoretically for long-range interactions in a lattice gas model at one-third filling [43], so far, the corresponding diagonal striped supersolid (dsSS) has been elusive on a square lattice (that is not subject to an external potential). Additionally, whether a cooperative electron-phonon interaction (that involves cooperative Jahn-Teller distortions) can explain the observed stripe charge order in LSNO is a controversial issue [44–46].

In the class of extended boson Hubbard models of the type $t_1 - t_2 - \dots - t_m - V_1 - V_2 - \dots - V_n$ [involving hoppings t_1, t_2, t_3 , etc., and interactions V_1, V_2, V_3 , etc., of ranges nearest neighbor (NN), next-nearest neighbor (NNN), next-to-next-nearest neighbor (NNNN), etc.] on a square lattice, the minimum model for realizing a checkerboard supersolid (cSS) is the $t_2 - V_1$ model [47,48]. It has also been shown that star/stripe supersolid [corresponding to crystalline ordering wave vector $(\pi, 0)$ or $(0, \pi)$] can be realized in a $t_1 - V_1 - V_2$ model; at one-fourth filling, a star solid results which is asymmetric with respect to doping with interstitials and vacancies [16]. Identifying the relevant extended boson Hubbard

model for obtaining the dsSS around one-third filling and characterizing the state are still open problems.

Here, inspired by the doped bismuthate systems, we develop a microscopic theory of HCBs strongly coupled to the cooperative breathing mode in a 2D perovskite lattice. The effective Hamiltonian for the HCBs is shown to be an extended boson Hubbard model of the form $t_1 - t_2 - t_3 - V_1 - V_2 - V_3$. The V_1 , V_2 , and V_3 repulsive interactions correspond to the minimum interactions needed to realize the diagonal striped order at one-third filling. Unlike many lattice models of the extended boson Hubbard type, the parameters (i.e., hopping term, strength of HCB-phonon coupling, and phonon frequency) in our $t_1 - t_2 - t_3 - V_1 - V_2 - V_3$ model either can be determined from band-structure calculations or can be obtained from experiments. Supersolidity in our model results only away from one-third filling and is shown to be asymmetric with respect to doping the commensurate diagonal-striped solid (dsS) with vacancies and interstitials. Although checkerboard supersolidity (away from half-filling) and diagonal striped supersolidity (away from one-third filling) are realized, there is no direct supersolid-supersolid phase transition between the two phases. We also show that our cooperative HCB-phonon framework can be extended to study charge order in LSNO; we demonstrate that the observed diagonal-stripe order at one-third filling and the checkerboard order at half-filling in LSNO can be explained by invoking cooperative Jahn-Teller effect.

The paper is organized as follows. In Sec. II, we derive an effective Hamiltonian of the system using a nonperturbative treatment. Next, in Sec. III we briefly describe the numerical procedure, as well as the quantities/parameters used in our study. Then, we discuss the results in Sec. IV, followed by a comparison with experimental observations in Sec. V. Finally, in Sec. VI, we conclude.

II. EFFECTIVE HAMILTONIAN

We start with a 2D model of HCBs depicted in Fig. 1. The HCBs interact with the in-plane (xy) oxygen atoms via CBM, whereas the nature of the interaction is noncooperative in the case of the out-of-plane oxygen atoms in the z direction. The Hamiltonian of such a system can be written as $H = H_t + H_l + H_i$, where the hopping term H_t is given by

$$H_t = -t \sum_{i,j} (d_{i+1,j}^\dagger d_{i,j} + d_{i,j+1}^\dagger d_{i,j} + \text{H.c.}), \quad (1)$$

with $d_{i,j}$ ($d_{i,j}^\dagger$) being the destruction (creation) operator of a HCB at the hopping site (i, j) and t being the hopping integral. The second term H_l in the Hamiltonian, which represents the HCB-phonon interaction, has the form

$$H_l = -g\omega_0 \sum_{i,j} [(a_{x;i,j}^\dagger + a_{x;i,j})(n_{i,j} - n_{i+1,j}) + (b_{y;i,j}^\dagger + b_{y;i,j})(n_{i,j} - n_{i,j+1}) + \gamma(c_{z;i,j}^\dagger + c_{z;i,j})n_{i,j}], \quad (2)$$

where $\gamma = \sqrt{2}$, g is the HCB-phonon coupling constant, and ω_0 is the optical-phonon frequency. The terms $(a_{x;i,j}^\dagger + a_{x;i,j})/\sqrt{2M\omega_0}$ and $(b_{y;i,j}^\dagger + b_{y;i,j})/\sqrt{2M\omega_0}$ denote the dis-

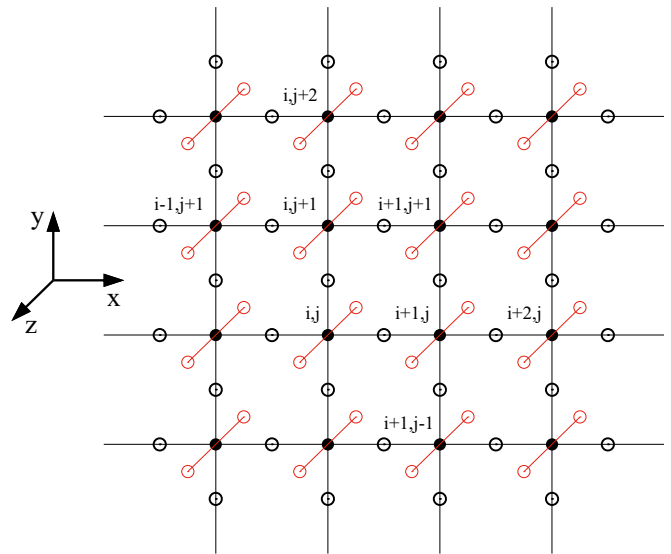


FIG. 1. Two-dimensional cooperative breathing mode (CBM) system with hopping sites of hard-core bosons (filled circles), in-plane oxygen atoms (black empty circles), and out-of-plane oxygen atoms (red empty circle). Only the in-plane oxygens are involved in cooperative distortions.

placement of the oxygen atom that is next to the (i, j) th hopping site and in the positive x and y directions, respectively; here, M is the mass of oxygen atom. The relative displacement of the two out-of-plane oxygens next to the (i, j) th site couples to the HCB at (i, j) th site and is denoted by $(c_{z;i,j}^\dagger + c_{z;i,j})/\sqrt{2\frac{M}{2}\omega_0}$ with $M/2$ being the reduced mass of the oxygen pairs. The expressions $(n_{i,j} - n_{i+1,j})$ and $(n_{i,j} - n_{i,j+1})$ in the first and second terms of Eq. (2) take care of the cooperative HCB-phonon interaction along the x and y directions, respectively. In the third term, note that we have only $n_{i,j}$ because of the noncooperative nature of the HCB-phonon interaction along the z direction. Furthermore, the last term in the Hamiltonian (i.e., the lattice term H_l), representing simple harmonic oscillators, is of the form

$$H_l = \omega_0 \sum_{i,j} (a_{x;i,j}^\dagger a_{x;i,j} + b_{y;i,j}^\dagger b_{y;i,j} + \eta c_{z;i,j}^\dagger c_{z;i,j}), \quad (3)$$

with $\eta = 1$. It is important to note that the above equation for the lattice term H_l treats the displacements $(a_{x;i,j}^\dagger + a_{x;i,j})/\sqrt{2M\omega_0}$ and $(b_{y;i,j}^\dagger + b_{y;i,j})/\sqrt{2M\omega_0}$ as independent variables; this is justified because these displacements depend on the site-occupancy differences $(n_{i,j} - n_{i+1,j})$ and $(n_{i,j} - n_{i,j+1})$, which are independent of each other. A similar consideration leads to a similar lattice term [given by Eq. (4)] in the treatment of cooperative Jahn-Teller distortions in Ref. [49].

We consider systems in the nonadiabatic regime ($t/\omega_0 \leq 1$) and strong-coupling region (large g^2). To produce an effective polaronic Hamiltonian, we employ a duality transformation where the strong-coupling problem in the original frame of reference [with small parameter $\alpha(g\omega_0)/t$] is transformed into a weak-coupling problem in a dual frame of reference [with small parameter $\alpha t/(g\omega_0)$, i.e., inverse of the small parameter in the original frame of reference]. To achieve the

above end, we need to modify the Lang-Firsov transformation [50] so as to take into account the cooperative nature of the distortions along the x and y directions and noncooperative nature in the z direction. This involves the following canonical transformation $\tilde{H} = \exp(S)H \exp(-S)$, where S is given by

$$S = -g \sum_{i,j} [(a_{x;i,j}^\dagger - a_{x;i,j})(n_{i,j} - n_{i+1,j}) + (b_{y;i,j}^\dagger - b_{y;i,j})(n_{i,j} - n_{i,j+1}) + \gamma(c_{z;i,j}^\dagger - c_{z;i,j})n_{i,j}]. \quad (4)$$

The transformed Hamiltonian can be written as $\tilde{H} = H_0 + H_1$, where the unperturbed Hamiltonian is given by

$$H_0 = \omega_0 \sum_{i,j} (a_{x;i,j}^\dagger a_{x;i,j} + b_{y;i,j}^\dagger b_{y;i,j} + \eta c_{z;i,j}^\dagger c_{z;i,j}) - E_p \sum_{i,j} n_{i,j} + 2V_p \sum_{i,j} (n_{i,j}n_{i+1,j} + n_{i,j}n_{i,j+1}) - te^{-(E_p+V_p)/\omega_0} \sum_{i,j} (d_{i+1,j}^\dagger d_{i,j} + d_{i,j+1}^\dagger d_{i,j} + \text{H.c.}), \quad (5)$$

and the perturbation by

$$H_1 = \sum_{i,j} H_{1i,j} = -te^{-(E_p+V_p)/\omega_0} \sum_{i,j} [d_{i+1,j}^\dagger d_{i,j} (\tau_{+x}^{ij} \tau_{-x}^{ij} - 1) + d_{i,j+1}^\dagger d_{i,j} (\tau_{+y}^{ij} \tau_{-y}^{ij} - 1) + \text{H.c.}], \quad (6)$$

where

$$\tau_{\pm x}^{ij} = \exp[\pm g(2a_{i,j} - a_{i-1,j} - a_{i+1,j}) \pm g(b_{i+1,j-1} + b_{i,j} - b_{i,j-1} - b_{i+1,j}) \pm \gamma g(c_{i,j} - c_{i+1,j})]$$

and

$$\tau_{\pm y}^{ij} = \exp[\pm g(2b_{i,j} - b_{i,j-1} - b_{i,j+1}) \pm g(a_{i-1,j+1} + a_{i,j} - a_{i-1,j} - a_{i,j+1}) \pm \gamma g(c_{i,j} - c_{i,j+1})].$$

Here, $E_p = (4 + \gamma^2)g^2\omega_0$ is the polaronic energy and $2V_p = 2g^2\omega_0$ represents the nearest-neighbor repulsion for the HCBs.

The eigenstates of the unperturbed Hamiltonian H_0 , relevant for perturbation theory, are $|n,m\rangle = |n\rangle_{\text{hcb}} \otimes |m\rangle_{\text{ph}}$, with $|0,0\rangle$ being the ground state with no phonons. The corresponding eigenenergies of such states are given by $E_{n,m} = E_n^{\text{hcb}} + E_m^{\text{ph}}$. Similar to the case of one-dimensional CBM model [51], we also have $\langle n,0|H_1|n,0\rangle = 0$, which yields the first-order perturbation term $\langle 0,0|H_1|0,0\rangle = 0$. In the region of interest in the parameter space, we note that $te^{-(E_p+V_p)/\omega_0} \ll \omega_0$; we perform second-order perturbation theory similar to that in the 1D CBM model [51] and obtain the effective Hamiltonian to be

$$H_{\text{eff}} = \langle 0|_{\text{ph}} H_0 |0\rangle_{\text{ph}} + H^{(2)}, \quad (7)$$

where

$$H^{(2)} = \sum_{i,j,k,l} \sum_m \frac{\langle 0|_{\text{ph}} H_{1i,j} |m\rangle_{\text{ph}} \langle m|_{\text{ph}} H_{1k,l} |0\rangle_{\text{ph}}}{E_0^{\text{ph}} - E_m^{\text{ph}}}. \quad (8)$$

One can easily see that the first term in H_{eff} is

$$\begin{aligned} \langle 0|_{\text{ph}} H_0 |0\rangle_{\text{ph}} &= -E_p \sum_{i,j} n_{i,j} + 2V_p \sum_{i,j} (n_{i,j}n_{i+1,j} + n_{i,j}n_{i,j+1}) \\ &\quad - te^{-(E_p+V_p)/\omega_0} \sum_{i,j} (d_{i+1,j}^\dagger d_{i,j} + d_{i,j+1}^\dagger d_{i,j} + \text{H.c.}), \quad (9) \end{aligned}$$

whereas the simplification of the second term (i.e., $H^{(2)}$) requires quite a bit of algebra. We extend the derivation of the effective Hamiltonian for the 1D CBM case [51] to our 2D case as well. As shown by using Schrieffer-Wolff transformation in Appendix A of Refs. [52,53], since $te^{-(E_p+V_p)/\omega_0} \ll \omega_0$, H_{eff} represents the exact Hamiltonian up to second order in perturbation. The small parameter here is given by $[\frac{t^2}{2(E_p+V_p)\omega_0}]^{\frac{1}{2}}$ whose derivation is similar to that in Ref. [54]. For the second term $H^{(2)}$ in H_{eff} , we obtain the terms given in the following sections.

A. Nearest-neighbor (NN) repulsion

The NN repulsion term comes from a process where a particle jumps to a neighboring site and comes back. In 2D, this term further consists of two parts: $\sum_{i,j} [n_{i,j}(1 - n_{i+1,j}) + n_{i+1,j}(1 - n_{i,j})]$ and $\sum_{i,j} [n_{i,j}(1 - n_{i,j+1}) + n_{i,j+1}(1 - n_{i,j})]$. Following a procedure explained in Appendix A, we get the expression for this process to be

$$-V_z \sum_{i,j} [n_{i,j}(1 - n_{i+1,j}) + n_{i,j}(1 - n_{i,j+1})], \quad (10)$$

with $V_z \approx \frac{2t^2}{2E_p+2V_p}$. The denominator $2E_p + 2V_p$ in V_z is the difference of the energy of the intermediate state (i.e., $E_p + 2V_p$ corresponding to the particle in the intermediate site) and the energy of the initial state ($-E_p$). The exact expression for V_z is derived in Appendix A.

B. Next-nearest-neighbor (NNN) and next-to-next-nearest-neighbor (NNNN) repulsions

We first make an important point while considering a process of a particle hopping to a neighboring site and coming back. In 2D, excluding the originating site, we must take into account the occupancy information about all the three remaining NN sites of the intermediate site of the hopping process. For example, consider a process where an HCB at site (i,j) hops to its neighboring site $(i+1,j)$ and comes back. For this process, we need to keep in mind the occupancy of the sites $(i+2,j)$, $(i+1,j+1)$, and $(i+1,j-1)$, which are the three relevant neighboring sites of the intermediate site $(i+1,j)$ (see Fig. 1). Depending on whether these sites are occupied or empty, the coefficient of the process will be modified accordingly. Essentially, there are four cases: (1) all the three NN sites are empty, (2) any one of the three neighboring sites

is occupied, (3) any two of the NN sites are occupied, and (4) all the three neighboring sites are occupied. Considering all the cases above, we end up with the following NNN and NNNN repulsion terms in $H^{(2)}$ as detailed in Appendix B.

1. NNN repulsion along diagonals

The first term is the NNN repulsion, which acts along the diagonals of the square lattice, and it is given by

$$V_2 \sum_{i,j} (n_{i,j} n_{i+1,j+1} + n_{i,j} n_{i-1,j+1}), \quad (11)$$

where

$$V_2 = 2t^2 \left[\left(\frac{1}{2} - m \right)^2 \frac{2V_p}{(E_p + V_p)(E_p + 2V_p)} + \left(\frac{1}{4} - m^2 \right) \frac{4E_p V_p}{(E_p + V_p)(E_p + 2V_p)(E_p + 3V_p)} + \left(\frac{1}{2} + m \right)^2 \frac{2E_p V_p}{(E_p + 2V_p)(E_p + 3V_p)(E_p + 4V_p)} \right], \quad (12)$$

with m being the magnetization of the system.

2. NNNN repulsion along the x and y axes

We find the second term to be the NNNN repulsion, which acts along the x and y axes of the square lattice; it is given by

$$V_3 \sum_{i,j} (n_{i,j} n_{i+2,j} + n_{i,j} n_{i,j+2}), \quad (13)$$

with $V_3 = \frac{V_z}{2}$. It is important to note that, in the absence of the NN repulsion $2V_p$, we obtain expressions for V_z , V_2 , and V_3 consistent with the noncooperative treatment of the electron-phonon interaction in Refs. [21,22].

C. NNN and NNNN hoppings

The remaining terms in $H^{(2)}$ are the hoppings of the HCBs to the NNN and NNNN sites. Similar to the NNN and NNNN repulsions, the hopping contributions of the HCBs can also be divided into two types: NNN hopping along the diagonals and NNNN hopping along the x and y axes (see Appendix C for details).

1. NNN hopping along diagonals

While calculating the coefficient of the NNN hopping, we have to keep in mind the fact that the HCB passes through an intermediate site while hopping to its NNN site. So the coefficient must depend on the occupancy of the two neighboring sites of the intermediate site. For example, if a HCB at site (i, j) is hopping to its right-upper diagonal site, i.e., $(i + 1, j + 1)$, it can follow any one of the two possible paths: (a) first going along x axis to the $(i + 1, j)$ th site and then along y axis to the $(i + 1, j + 1)$ th site; and (b) the interchanged process, i.e., hopping along the y axis first to the $(i, j + 1)$ th site followed by a hop along the x axis to the $(i + 1, j + 1)$ th site (see Fig. 1). For the first path, the coefficient of the hopping depends on whether the two sites $(i + 2, j)$ and $(i + 1, j - 1)$, which are NN of the intermediate

site $(i + 1, j)$, are occupied or empty. On the other hand, for the second path, the hopping coefficient depends on the occupancy of the two neighboring sites of the intermediate site $(i, j + 1)$, i.e., $(i - 1, j + 1)$ and $(i, j + 2)$. To calculate the NNN hopping coefficient, first we forget about the occupancy of the two neighbors of the intermediate site; then, the NNN hopping along the diagonals is obtained to be

$$- \frac{2t^2 e^{-E_p/\omega_0}}{E_p + 2V_p} \sum_{i,j} (d_{i+1,j+1}^\dagger d_{i,j} + d_{i-1,j+1}^\dagger d_{i,j} + \text{H.c.}), \quad (14)$$

where the coefficient $\frac{2t^2 e^{-E_p/\omega_0}}{E_p + 2V_p}$ is an approximation with the exact expression being given in Appendix C.

Now, taking the two neighbors of the intermediate site into account, the NNN hopping term along the diagonals of the square lattice gets modified to be

$$-t_2 \sum_{i,j} (d_{i+1,j+1}^\dagger d_{i,j} + d_{i-1,j+1}^\dagger d_{i,j} + \text{H.c.}), \quad (15)$$

where

$$t_2 = \frac{2t^2 e^{-E_p/\omega_0}}{E_p + 2V_p} \left[\left(\frac{1}{2} - m \right)^2 + \left(\frac{1}{4} - m^2 \right) \frac{2E_p + 4V_p}{E_p + 4V_p} + \left(\frac{1}{2} + m \right)^2 \frac{E_p + 2V_p}{E_p + 6V_p} \right]. \quad (16)$$

2. NNNN hopping along the x and y axes

Next, we consider the hopping of the HCBs to the NNNN sites along the x and y axes of the square lattice. Similar to the previous case, the coefficient of the hopping in this case, depends on the occupancy of the two neighboring sites of the intermediate site. For example, if a HCB is hopping from site (i, j) to its NNNN site $(i + 2, j)$, it has to pass through the intermediate site $(i + 1, j)$ (see Fig. 1). So, the coefficient for this process depends on whether the neighboring sites of site $(i + 1, j)$, i.e., $(i + 1, j + 1)$ and $(i + 1, j - 1)$, are occupied or empty. Taking into account all the occupancy possibilities of the neighboring sites of the intermediate site, we get the NNNN hopping term to be

$$-t_3 \sum_{i,j} (d_{i+2,j}^\dagger d_{i,j} + d_{i,j+2}^\dagger d_{i,j} + \text{H.c.}), \quad (17)$$

with $t_3 = \frac{t_2}{2}$. Again, it should be pointed out that, in the absence of the NN repulsion $2V_p$, the expressions for t_2 and t_3 simplify to be consistent with the results of the noncooperative analysis of the electron-phonon interaction in Refs. [21,22].

Finally, taking all the terms present in $H^{(2)}$ into account, H_{eff} in Eq. (7) reduces to

$$H_{\text{eff}} = -(E_p + 2V_z) \sum_{i,j} n_{i,j} - t_1 \sum_{i,j} (d_{i+1,j}^\dagger d_{i,j} + d_{i,j+1}^\dagger d_{i,j} + \text{H.c.}) + V_1 \sum_{i,j} (n_{i,j} n_{i+1,j} + n_{i,j} n_{i,j+1}) - t_2 \sum_{i,j} (d_{i+1,j+1}^\dagger d_{i,j} + d_{i-1,j+1}^\dagger d_{i,j} + \text{H.c.})$$

$$\begin{aligned}
& + V_2 \sum_{i,j} (n_{i,j} n_{i+1,j+1} + n_{i,j} n_{i-1,j+1}) \\
& - t_3 \sum_{i,j} (d_{i+2,j}^\dagger d_{i,j} + d_{i,j+2}^\dagger d_{i,j} + \text{H.c.}) \\
& + V_3 \sum_{i,j} (n_{i,j} n_{i+2,j} + n_{i,j} n_{i,j+2}), \quad (18)
\end{aligned}$$

where $t_1 = t e^{-(E_p + V_p)/\omega_0}$, $V_1 = 2V_p + V_z$, and the expressions for all the remaining terms, V_z , t_2 , t_3 , V_2 , and V_3 , being the same as defined earlier.

III. NUMERICAL CALCULATIONS

To study the phase diagram of our effective Hamiltonian of HCBs, we use quantum Monte Carlo (QMC) simulation adopting the stochastic-series-expansion (SSE) technique [55,56]; furthermore we employ directed loop update [57,58]. We find it convenient to rewrite the Hamiltonian in terms of spin-1/2 operators. Identifying the relations between the operators for HCBs and those for spin-1/2 particles as $d_{i,j}^\dagger = S_{i,j}^+$, $d_{i,j} = S_{i,j}^-$, and $n_{i,j} = S_{i,j}^z + \frac{1}{2}$, we recast our effective Hamiltonian for HCBs, in units of $2t_1$, as an extended XXZ spin-1/2 Hamiltonian, given by

$$\begin{aligned}
H = \sum_{i,j} & \left[-\frac{1}{2} (S_{i+1,j}^+ S_{i,j}^- + S_{i,j+1}^+ S_{i,j}^- + \text{H.c.}) \right. \\
& \left. + \Delta_1 (S_{i,j}^z S_{i+1,j}^z + S_{i,j}^z S_{i,j+1}^z) \right] \\
& + \sum_{i,j} \left[-\frac{J_2}{2} (S_{i+1,j+1}^+ S_{i,j}^- + S_{i-1,j+1}^+ S_{i,j}^- + \text{H.c.}) \right. \\
& \left. + \Delta_2 (S_{i,j}^z S_{i+1,j+1}^z + S_{i,j}^z S_{i-1,j+1}^z) \right] \\
& + \sum_{i,j} \left[-\frac{J_3}{2} (S_{i+2,j}^+ S_{i,j}^- + S_{i,j+2}^+ S_{i,j}^- + \text{H.c.}) \right. \\
& \left. + \Delta_3 (S_{i,j}^z S_{i+2,j}^z + S_{i,j}^z S_{i,j+2}^z) \right] - h_0 \sum_{i,j} S_{i,j}^z. \quad (19)
\end{aligned}$$

Looking at Eqs. (18) and (19), one can easily see that $J_2 = t_2/t_1$, $J_3 = t_3/t_1$, $\Delta_1 = V_1/(2t_1)$, $\Delta_2 = V_2/(2t_1)$, $\Delta_3 = V_3/(2t_1)$, and $h_0 = E_p + 2V_z - 2V_1 - 2V_2 - 2V_3$; here, J_i and Δ_i are the transverse and longitudinal couplings, respectively.

Now, to figure out the phase diagram of the system, we need to study the Hamiltonian at various filling-fractions of HCBs. To vary the number of HCBs in the system, or in other words to tune the magnetization of the spin-1/2 system, we replace the constant h_0 by a variable h in the term $-h_0 \sum_{i,j} S_{i,j}^z$ of the Hamiltonian H given by Eq. (19); here, h is taken as the external magnetic field in units of $2t_1$. By tuning the external magnetic field h , we can actually tune the magnetization of the system and study the behavior of the system at various fillings.

To capture the ground-state properties of a $L \times L$ square lattice using SSE, the simulations should be done at low enough temperatures, i.e., the inverse temperature $\beta \sim L$ [59].

For our Hamiltonian, since the numerical calculations for $\beta = 3L/2$ and $\beta = 2L$ produce same results within the error bars of our calculations, we present the results for $\beta = 3L/2$.

We use two kinds of order parameter: structure factor $S(\vec{Q})$ (to identify diagonal long-range order) and superfluid density ρ_s (to identify off-diagonal long-range order) and construct the phase diagram. The structure factor per site is defined as

$$S(\vec{Q}) = \frac{1}{N_s^2} \sum_{i,j} \sum_{m,n} e^{i\vec{Q} \cdot (\vec{R}_{i,j} - \vec{R}_{m,n})} \langle S_{i,j}^z S_{m,n}^z \rangle, \quad (20)$$

with $\langle \dots \rangle$ being the ensemble average. We study $S(\vec{Q})$ at all values of \vec{Q} and identify those that produce peaks in the structure factor. Here we would like to point out that the maximum possible value of $S(\vec{Q})$ is 0.25.

The superfluid density is expressed in terms of the winding numbers, W_x and W_y , in the x and y directions as [56]

$$\rho_s = \frac{1}{2\beta} (W_x^2 + W_y^2). \quad (21)$$

The winding number W_x along the x direction can be calculated as $W_x = \frac{1}{L_x} (N_x^+ - N_x^-)$, where N_x^+ and N_x^- denote the total number of operators transporting spin in positive and negative x directions, respectively, and L_x denotes the length of the lattice along the x direction.

We now discuss the values of different parameters in our Hamiltonian given by Eq. (19) and used in our numerical calculations. We concentrate on the case $t/\omega_0 = 1.0$ for the construction of our phase diagram. Since $\gamma = \sqrt{2}$, we set $\tilde{g}^2 = 7g^2$ so as to get the simple expression $E_p + V_p = \tilde{g}^2 \omega_0$. The coefficients $J_2 (= 2J_3)$ and $\Delta_2 (= 2\Delta_3)$ depend on the magnetization m of the system. While Fig. 2 depicts that J_2

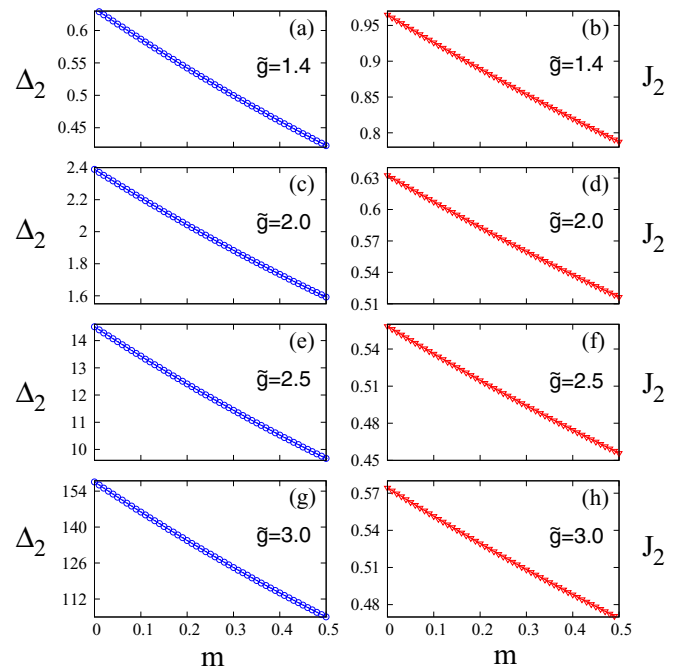


FIG. 2. Dependence of NNN longitudinal coupling Δ_2 and NNN transverse coupling J_2 on magnetization m as derived from Eqs. (12), (16), (18), and (19) for the following cases: (a) and (b) at $\tilde{g} = 1.4$, (c) and (d) at $\tilde{g} = 2.0$, (e) and (f) at $\tilde{g} = 2.5$, and (g) and (h) at $\tilde{g} = 3.0$.

TABLE I. Values of NN longitudinal coupling Δ_1 and maximum values of NNN longitudinal coupling Δ_2 and NNN transverse coupling J_2 for different values of \tilde{g} .

\tilde{g}	Δ_1	$(\Delta_2)_{\max}$	$(J_2)_{\max}$
1.0	1.7436	0.4757	1.6486
1.5	5.7744	0.7379	0.8760
1.8	16.6463	1.3791	0.7007
2.0	39.2161	2.3887	0.6327
2.25	131.8584	5.4612	0.5818
2.5	507.9968	14.5044	0.5584
3.0	10896.8217	157.5599	0.5744

and Δ_2 values (at various couplings \tilde{g}) monotonically decrease with increasing magnetization m , Table I shows the values of Δ_1 and the maximum values of Δ_2 and J_2 for different values of \tilde{g} . As one can see, $\Delta_1/(\Delta_2)_{\max}$ increases monotonically approximately from 3.665 to 69.159 as \tilde{g} is varied from 1.0 to 3.0. At larger values of \tilde{g} , when Δ_1 and Δ_2 assume large values, our numerical calculations suffer from significant slowing down resembling the situation in Ref. [21]; with our computational constraints we cannot use exact values when Δ_1 and Δ_2 assume large values. We can set a cutoff for the parameters Δ_1 and Δ_2 above which the essential physics for our system remains unaltered. Similar to Ref. [21], the upper cutoff for Δ_1 is 16. Furthermore, to identify the cutoff for Δ_2 , we need to find out the lowest value of Δ_1/Δ_2 which can be used without changing the essential physics. To this end, we have calculated the superfluid density and structure factor at half-filling (where $\Delta_2 = (\Delta_2)_{\max}$) for the following set of values of $(\Delta_1, (\Delta_2)_{\max})$: (20,4), (20,5), (20,6), (16,5), (20,7), (17,6), (16,7), and (20,9) with the value of $\Delta_1/(\Delta_2)_{\max}$ being 5, 4, 3.33, 3.2, 2.86, 2.83, 2.29, and 2.22, respectively. Numerical results show that for the first four cases, where $\Delta_1 > 3(\Delta_2)_{\max}$, at half-filling, the system manifests a checkerboard solid (cS) with a peak in the structure factor $S(\pi, \pi)$. On the other hand, for the last four cases where $2(\Delta_2)_{\max} < \Delta_1 < 3(\Delta_2)_{\max}$, at half-filling, the system produces a completely different type of solid depicted in Fig. 3 (which we call honeycomblike solid), indicated by a peak in $S(\pi/2, \pi)$ or $S(\pi, \pi/2)$. The reason can be explained as follows. In the cS phase, each particle feels $6(\Delta_2)_{\max}$ amount repulsion, whereas in the honeycomblike solid the repulsion felt by each particle is $\Delta_1 + 3(\Delta_2)_{\max}$. The checkerboard solid will be favored over the honeycomblike solid only if $\Delta_1 + 3(\Delta_2)_{\max} > 6(\Delta_2)_{\max}$,

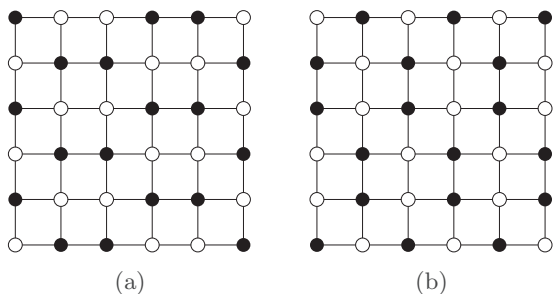


FIG. 3. Two types of honeycomblike solid depicted by a peak in (a) $S(\pi/2, \pi)$ and (b) $S(\pi, \pi/2)$.

TABLE II. Autocorrelation times measured for $\tilde{g} = 2.5$ using $\epsilon_1 = 8$, $\epsilon_2 = 5/4$, and $\epsilon_3 = \epsilon_2/2$; chosen magnetic fields are in the vicinity of the transitions as well as away from the transitions (see Fig. 8 for details).

h	5.0	13.0	15.35	29.50	34.0
τ_{int}	279692	55792	147933	192790	5747

i.e., $\Delta_1 > 3(\Delta_2)_{\max}$. Therefore, to capture the correct physics of our system, the minimum value of Δ_1/Δ_2 must be greater than 3. Keeping all these facts in mind, we set the cutoff values to be $\Delta_1 = 16$ and $\Delta_2 = 5$ (with $\Delta_3 = \frac{\Delta_2}{2}$), so that the physics of the system still remains the same.

As discussed in Ref. [21], it is important to mention here that the parameter ϵ_i (see Appendix D for details), introduced to make the two-spin matrix elements positive, can affect the autocorrelation time especially for large anisotropies (i.e., large values of Δ_1 , Δ_2 and Δ_3). To ensure that the autocorrelation time is much smaller than the bin size used to calculate the observables (in all the cases considered), we compute the autocorrelation time τ_{int} given by the following formula:

$$\tau_{\text{int}}[m] = \frac{1}{2} + \sum_{t=1}^{\infty} A_m(t) \quad (22)$$

with

$$A_m(t) = \frac{\langle m(i+t)m(i) \rangle - \langle m(i) \rangle^2}{\langle m(i)^2 \rangle - \langle m(i) \rangle^2}, \quad (23)$$

where i and t represent Monte Carlo sweeps and $\langle \dots \rangle$ denotes average over the time i . Based on our autocorrelation data, we observe that when $\Delta_i \leq 10$, taking $\epsilon_i = \Delta_i/4$ is good enough to keep the autocorrelation time much smaller than the bin size. Given the cutoff values of Δ_2 and Δ_3 mentioned above, we always take $\epsilon_2 = \Delta_2/4$ and $\epsilon_3 = \Delta_3/4$. On the other hand, as Δ_1 increases from 10 to 16 (i.e., cutoff value of Δ_1), ϵ_1 is taken to steadily increase from $\Delta_1/4$ (i.e., 2.5) to $\Delta_1/2$ (i.e., 8). To give an estimate of the autocorrelation time at large Δ_1 values, Table II shows the autocorrelation times for $\tilde{g} = 2.5$ at magnetic fields chosen in the vicinity of the phase transitions (where the autocorrelation time is expected to be large) as well as in regions far from the transitions. In Table II, the magnetic field $h = 5.0$ corresponds to a point in the cSS region close to the cSS-SF transition; whereas $h = 15.35$ and 29.50 represent points in the dsSS region in the vicinity of the dsSS-SF transition (see Fig. 8). On the other hand, $h = 13.0$ and 34.0 correspond to two points in the SF region away from the transitions. The values of the autocorrelation time τ_{int} (listed in Table II) clearly show that close to the transitions the autocorrelation time increases significantly, whereas it remains comparatively small in the regions away from the transitions. The bin size used for all calculations is 20 00 000; this ensures that τ_{int} is well within the bin size.

All numerical results in Figs. 4–11 have been obtained on an 18×18 lattice with $t/\omega_0 = 1.0$. Furthermore, along with the 18×18 phase diagram, in Fig. 6, the phase boundaries for a 12×12 lattice are also plotted.

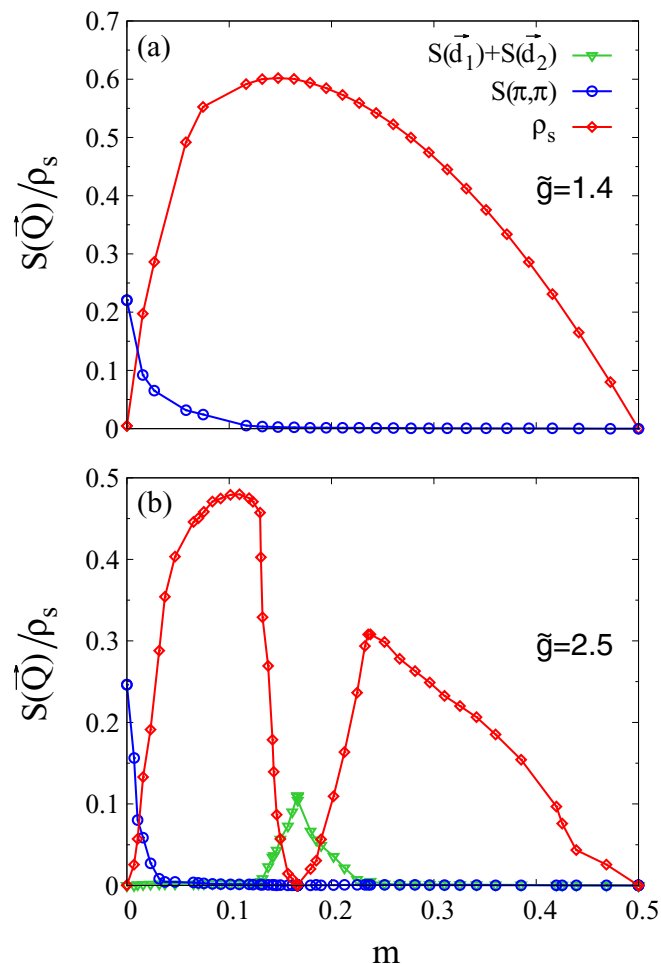


FIG. 4. Plots of structure factor $S(\vec{Q})$ and superfluid density ρ_s vs magnetization m for HCBs on a 18×18 lattice with $t/\omega_0 = 1.0$ and when (a) $\tilde{g} = 1.4$ and (b) 2.5. Curves are averaged results from simulations using three different random number seeds.

IV. RESULTS AND DISCUSSIONS

To determine the various phases of our 2D $t_1 - t_2 - t_3 - V_1 - V_2 - V_3$ model, one needs to understand the interplay between different types of hopping and repulsion. To construct the phase diagram, we vary the magnetization m from 0 to 0.5; this corresponds to varying the particle filling ρ from 1/2 to 1. Due to the particle-hole symmetry of the Hamiltonian, the physics at any filling fraction for particles is identical to that for holes at the same filling.

Figure 4 shows the variation of the structure factor $S(\vec{Q})$ and the superfluid density ρ_s as a function of the magnetization m , for two different values of \tilde{g} , i.e., 1.4 and 2.5. A key point to note here is that, in general, larger values of repulsion aid in the formation of a CDW, whereas larger values of NNN tunneling t_2 help a particle hop in the same sublattice. For $\tilde{g} = 1.4$, at half-filling, the HCBs form a checkerboard solid shown in Fig. 5(a) and indicated by a peak in the structure factor $S(\pi, \pi)$. Slightly away from half-filling, a supersolid region develops after which the system retains only its superfluidity. The reason can be understood by examining the coefficients of different terms in the Hamiltonian in Eq. (19). Since the NN

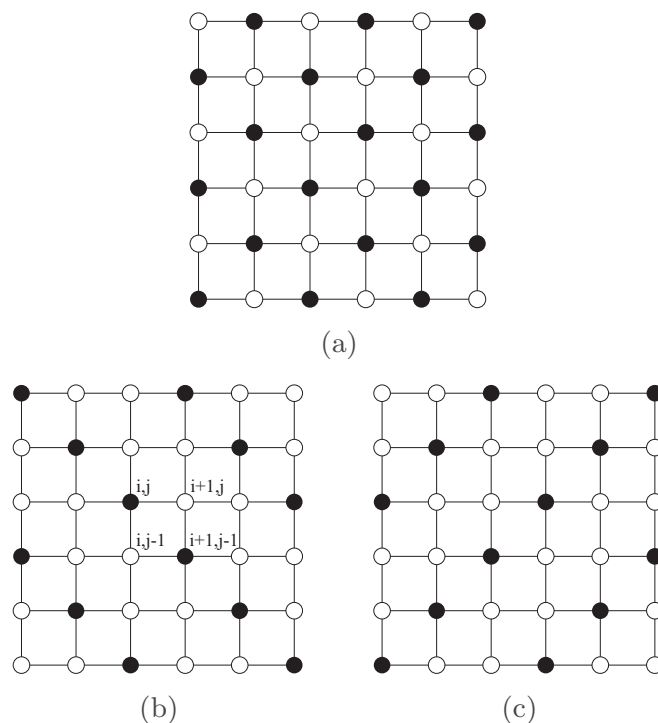


FIG. 5. Different types of CDWs: (a) checkerboard solid (cS) at half-filling with $S(\vec{Q})$ peaking at $\vec{Q} = (\pi, \pi)$; (b) diagonal striped solid (dsS) indicated by peak in $S(\vec{Q})$ at $\vec{Q} = (2\pi/3, 2\pi/3)$; and (c) dsS characterized by ordering wave vector $\vec{Q} = (2\pi/3, 4\pi/3)$.

repulsion dominates over the NNN and NNNN repulsions, at half-filling the system becomes a cS phase to avoid NN occupation, even though the particles experience NNN and

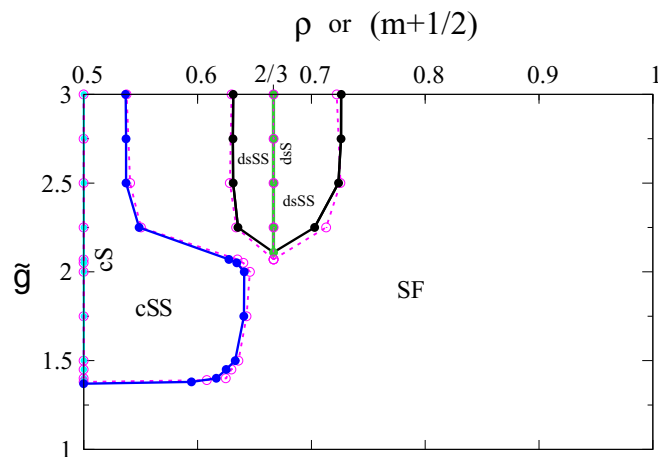


FIG. 6. Phase diagram in terms of filling fraction ρ (or magnetization m) for HCBs on a 12×12 and 18×18 lattice with $t/\omega_0 = 1.0$. The magenta dashed lines and open circles represent the phase boundaries for the 12×12 system, whereas the boundaries for the 18×18 lattice are depicted by the solid lines and filled circles (i.e., in cyan, blue, black, and green colors). Here, cS represents a checkerboard solid with cSS being the corresponding supersolid; dsS stands for diagonal striped solid with dsSS being the related supersolid. Plots represent averaged results from simulations employing three different random number seeds.

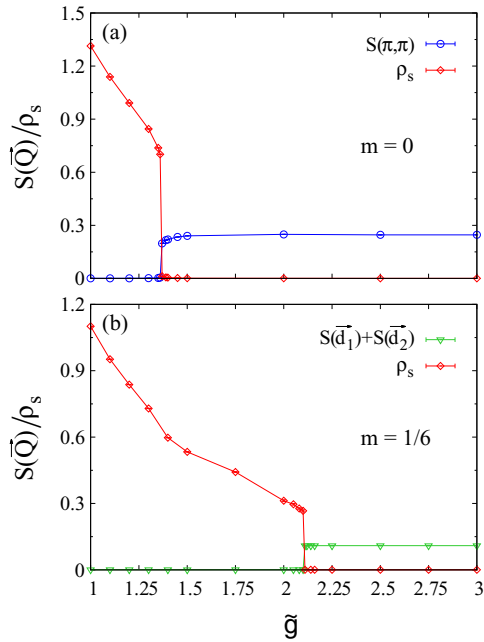


FIG. 7. Plots of $S(\vec{Q})$ and ρ_s vs coupling strength \tilde{g} depicting first-order transitions at two different magnetization values: (a) $m = 0$ (or half-filling) and (b) $m = 1/6$ (or two-third filling).

NNNN repulsions. Now, if we add one additional particle to the half-filled system, the extra particle can be at any one of the empty sites; irrespective of the site it resides on, the particle will feel the same extra repulsion $4V_1$. This extra particle can hop to its NNN or NNNN sites, without changing the repulsive interaction in the system that has a checkerboard solid in the background, resulting in the coexistence of superfluidity and CDW state. If we keep on increasing the particle number, after a certain filling fraction, the checkerboard structure is lost with the system continuing to be a superfluid.

Now looking at Fig. 4(b) for $\tilde{g} = 2.5$, we see that an additional CDW appears at fillings $\rho = 1/3$ and $2/3$. Since the physics pertinent to $\rho = 1/3$ is the same as that for

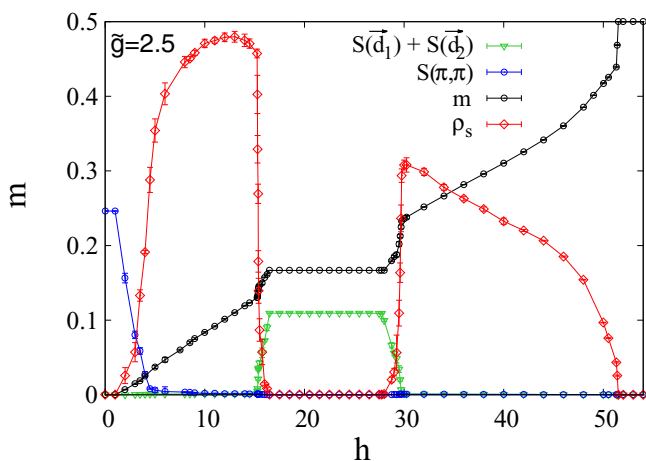


FIG. 8. Evolution of order parameters $S(\vec{Q})$, ρ_s , and m as the magnetic field h is varied at a fixed coupling strength $\tilde{g} = 2.5$. No discontinuous transitions are exhibited.

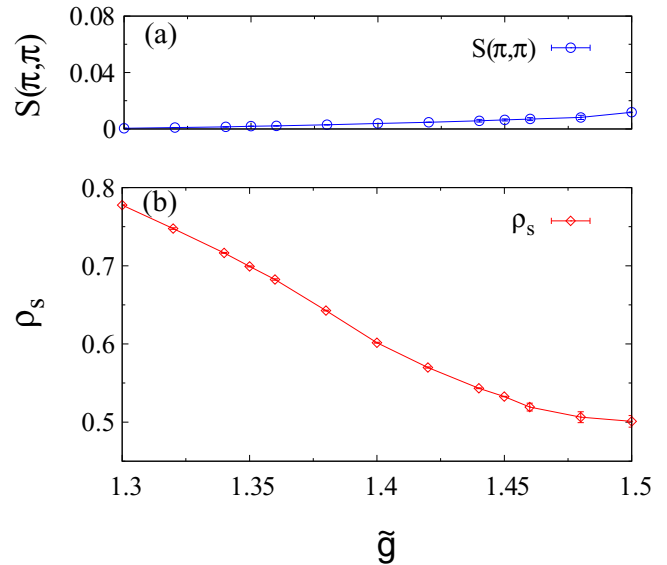


FIG. 9. Plots of (a) $S(\pi, \pi)$ and (b) ρ_s vs coupling strength \tilde{g} , at density $\rho = 0.61635 \pm 0.00007$, depicting a continuous transition from SF to cSS phase as we increase the \tilde{g} value.

$\rho = 2/3$, we will analyze them interchangeably based on our convenience. At $\rho = 1/3$, the HCBs form a diagonal striped solid manifesting spontaneously broken symmetry and characterized by a peak in the structure factor at wave vector $\vec{d}_1 = (2\pi/3, 2\pi/3)$ [corresponding to Fig. 5(b)] or $\vec{d}_2 = (2\pi/3, 4\pi/3)$ [related to Fig. 5(c)]. Although each particle in the stripe experiences a repulsion $2V_2$, it is still the minimum energy state of the system at one-third filling. If we add one extra particle to the system, it occupies any one of the empty sites between the stripes and experiences a repulsion $2V_1 + V_2 + 2V_3$. Now, this extra particle can hop to any of its unoccupied NN, NNN, or NNNN sites without a change in the potential energy of the system; thus, coexistence of stripe order and superfluidity is realized on the interstitial side. On the other hand, if we remove one particle from the system at $\rho = 1/3$, the extra hole (residing in the stripes) can hop

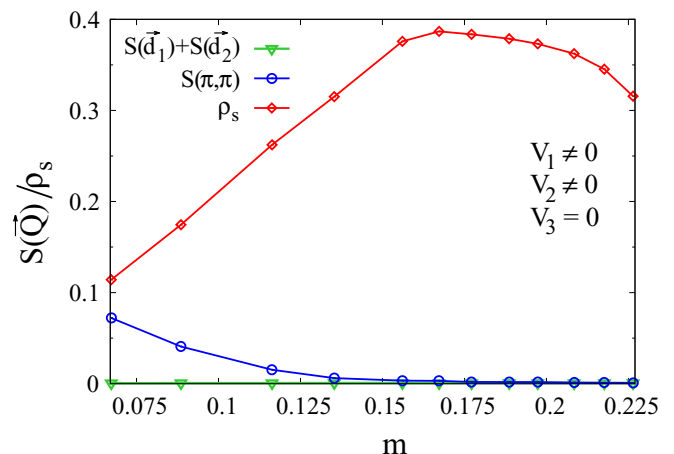


FIG. 10. Variation of $S(\vec{Q})$ and ρ_s vs magnetization m in the absence of the NNNN repulsion V_3 along x- and y-axes in the $t_1 - t_2 - t_3 - V_1 - V_2 - V_3$ model of Eq. (18).

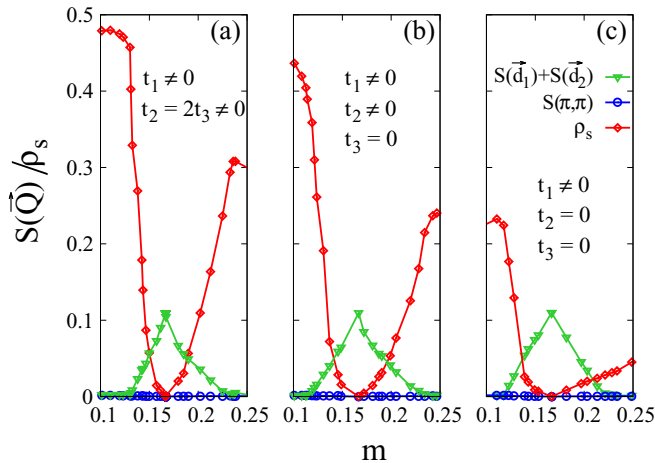


FIG. 11. Plots of $S(\vec{Q})$ and ρ_s vs magnetization m , in the vicinity of striped phase, for three different cases in the $t_1 - t_2 - t_3 - V_1 - V_2 - V_3$ model of Eq. (18): (a) all the three hoppings t_1 , t_2 , and t_3 are present, (b) NNNN hopping t_3 along x and y axes is set to zero, and (c) only NN hopping t_1 is present. The minimum model for diagonal striped solid (dsS) is shown to be $t_1 - V_1 - V_2 - V_3$.

along the stripes without altering the potential energy; thus, supersolidity is exhibited on the other (i.e., vacancy) side of the diagonal striped phase as well. Thus the mechanism governing the existence of a supersolid phase away from commensurate fillings $1/2$ and $1/3$, on our unfrustrated system (i.e., the square lattice), is that interstitials or vacancies can move without frustration, i.e., without a cost in the potential energy.

The complete ground-state phase diagram is depicted in Fig. 6 for 12×12 and 18×18 square lattices; we see that the phase diagram is by and large independent of the system size for $6L \times 6L$ square lattices when $L \geq 2$. It should be noted that, for $L \geq 4$, the simulation times are prohibitively large at large repulsions (or anisotropies). We will now proceed to discuss the phase diagram for the 18×18 lattice. The half-filled system shows the signature of a checkerboard solid (cS) for all \tilde{g} values above 1.37. Next to this CDW, we have a supersolid region (cSS) where $S(\pi, \pi)$ and ρ_s coexist homogeneously. On the other hand, at filling fraction $\rho = 1/3$, the system realizes a dsS beyond $\tilde{g} = 2.11$. On both sides of this striped solid, we have a region of supersolid (dsSS), which is a homogeneous coexistence of the diagonal striped solid and a superfluid. As we increase \tilde{g} beyond 1.37, the width of the supersolid region cSS increases and attains its maximum at $\tilde{g} = 2.0$. Further increase in \tilde{g} results in a decrease in the width of the cSS region, thereby making way for diagonal stripe supersolid at higher values of \tilde{g} . However, we should point out that there is no direct supersolid-supersolid transition. Next, it is interesting to note that there is an asymmetry in the extent of the dsSS region around one-third filling. Thus there is an asymmetry at $\rho = 1/3$ with respect to doping with interstitials and vacancies similar to the asymmetry at one-fourth filling reported in Ref. [16] for a $t_1 - V_1 - V_2$ model when $V_1 < 2V_2$. It is also worth noting that, at lower fillings such as $\rho = 1/4$ and $\rho = 1/5$, there is no CDW order.

In a recent study of HCBs on a square lattice with NN hopping and NN repulsion (i.e., in a $t_1 - V_1$ model), when a

sizable external potential is applied along the diagonal stripes in Figs. 5(b) and 5(c), the authors obtain the corresponding diagonal striped CDW at $\rho = 1/3$ and a striped supersolid phase away from one-third filling [60]. Similar to our case, the physics governing the formation of a supersolid phase is that the interstitial particles or vacancies in the vicinity of the commensurate filling $\rho = 1/3$ can hop without changing the potential energy of the system.

In our simulations using SSE, we cannot tune the magnetization (density) directly. Instead, we tune the magnetic field which determines the magnetization of the system. For a particular value of the magnetic field, the resulting magnetization generally fluctuates during simulation. As a result, usually it is not possible to study the nature of the phase transitions by keeping the magnetization (filling-fraction) fixed at a particular value and varying \tilde{g} . However, when the system is in a CDW state, the magnetization remains constant over a range of magnetic field values; this makes it possible to vary \tilde{g} at a fixed magnetization.

We see from Fig. 7(a) that for the half-filled system (i.e., at $m = 0$), as we increase the \tilde{g} value from 1 to 3, the structure factor $S(\pi, \pi)$ jumps from 0 to almost its maximum value and the superfluid density suddenly drops down to zero at $\tilde{g} = 1.37$. In the phase diagram (depicted in Fig. 6), this indicates a first-order transition at $\tilde{g} = 1.37$ from a superfluid to a checkerboard solid at filling fraction $1/2$; since the transition is from a U(1) symmetry breaking state to a translational symmetry breaking state, the order of the transition is consistent with Landau's picture. Furthermore, our observation of discontinuous transition from a superfluid to checkerboard solid is also consistent with the results of Refs. [31,61]. Similarly, at magnetization $m = 1/6$ corresponding to filling fraction $2/3$, at $\tilde{g} = 2.11$, Fig. 7(b) shows a dramatic jump in the structure factor $S(2\pi/3, 2\pi/3) + S(2\pi/3, 4\pi/3)$ from 0 to its maximum value accompanied by a discontinuous drop in the superfluid density to zero. This signifies a first-order transition as we move along the \tilde{g} -axis at $m = 1/6$ in the phase diagram (shown in Fig. 6). Thus, consistent with the literature [16,18,62], no supersolidity is detected at commensurate fillings in our unfrustrated system. Here it should be pointed out that in Fig. 7(a) and 7(b), after the transition from superfluid to CDW (cS and dsS) state, the magnetizations can be fixed exactly at $m = 0$ and $1/6$, respectively. However, before the transitions, i.e., in the superfluid region, the magnetizations are given by $m = 0 \pm 0.0000006$ and $1/6 \pm 0.00002$.

Next, away from the special points [63] ($\rho = 0.5, \tilde{g} = 1.37$) and ($\rho = 2/3, \tilde{g} = 2.11$), we will study the nature of the transitions as a function of the magnetization. As seen in Fig. 4, the order parameters change continuously, upon tuning the magnetization of the system at a fixed \tilde{g} value, signifying continuous phase transitions between different phases. A more reliable indicator, to detect the nature of the phase transitions along the ρ axis of the phase diagram, is the behavior of the order parameters (i.e., magnetization, superfluid density and structure factor) as the magnetic field h is varied. In Fig. 8, the continuous variation of the order parameters as a function of the magnetic field h clearly eliminates the possibility of a first-order phase transition. Therefore, in the phase diagram displayed in Fig. 6, as we move along the ρ axis at any particular \tilde{g} value, all the different phases are separated from

each other via continuous phase transitions, i.e., all supersolid-solid and superfluid-supersolid transitions are continuous.

As mentioned earlier, at a fixed magnetization, it is difficult to analyze the transition between the superfluid and the supersolid phases as a function of \tilde{g} . Now, it is expected that the nature of the transition between the two phases is independent of whether it is driven by the coupling or the density. To demonstrate this, we concentrate on the phase transition between SF and cSS. From the phase diagram in Fig. 6, we see that around $\rho \approx 0.616$, a phase transition takes place between SF and cSS as \tilde{g} is varied from 1.35 to 1.40. Therefore, for a number of \tilde{g} values ranging from 1.3 to 1.5, we have varied the magnetic field (in very small steps) so as to obtain the density ρ as close as possible to 0.616 for each \tilde{g} . Figure 9 shows the behavior of $S(\pi, \pi)$ and ρ_s as a function of \tilde{g} at density $\rho = 0.61635 \pm 0.00007$. The smooth variation of the order parameters suggest that the nature of the transition between superfluid (SF) and checkerboard supersolid (cSS) is continuous as we move along the \tilde{g} axis in the phase diagram. Similarly, we expect the nature of the transition to be also continuous between the superfluid (SF) and diagonal striped supersolid (dsSS) phases as we tune the \tilde{g} value.

We will now identify the minimum model for the diagonal striped supersolid. Compared to the checkerboard supersolid, the dsSS phase is rarely observed. To determine the minimum model for the realization of the dsSS phase, we first identify the necessary repulsions required to observe the diagonal striped solid phase in the $t_1 - t_2 - t_3 - V_1 - V_2 - V_3$ model of Eq. (18). From Fig. 10, we see that, as soon as we tune the NNNN repulsion V_3 along x and y axes to zero, the structure factor corresponding to the dsS phase completely disappears. This feature can be explained based on Figs. 5(b) and 5(c). For instance, when the NNNN repulsion V_3 is set to zero in the structure given by Fig. 5(b), the particles at sites (i, j) and $(i + 1, j - 1)$ can both be shifted to the neighboring sites $(i + 1, j)$ and $(i, j - 1)$ without changing the potential energy of the system. This process destroys the striped structure. Thus it follows that all the three repulsions (i.e., V_1 , V_2 , and V_3) are necessary to stabilize the dsS structure. A similar argument can be made to destroy the structure given by Fig. 5(c).

Next, in Fig. 11, we focus on the region in the vicinity of the striped phase. Compared to Fig. 11(a), in which all the three hopping parameters are nonzero, the superfluid density reduces slightly when the NNNN hopping t_3 is set to zero [as can be seen in Fig. 11(b)]. The interesting feature to note is that, even when only NN hopping t_1 is present with the other two hopping parameters t_2 and t_3 being zero [as in Fig. 11(c)], we have a diagonal striped supersolid region around $m = 1/6$ with the width of the dsSS being almost unaffected. This elucidates the fact that the minimum model to obtain a dsSS phase is the $t_1 - V_1 - V_2 - V_3$ model.

V. COMPARISON WITH LSNO EXPERIMENTAL RESULTS

Stripelike charge order has been reported in a number of layered transition-metal oxides [36]. Among these compounds, the layered nickelate LSNO is an archetypal system to exhibit a firm charge stripe order. In $\text{La}_{2-x}\text{Sr}_x\text{NiO}_4$, static checkerboard charge order [such as in Fig. 5(a)] is expressed at $x = 1/2$ and static diagonal stripe order [as shown in Figs. 5(b) and 5(c)] is

manifested at $x = 1/3$ with the transition temperatures at these dopings showing local maxima [37–42]. The observed lattice constant ratio c/a in LSNO displays a maximum at $x = 1/2$, thereby indicating that in the region $0 < x < 1/2$ holes are doped into the $d_{x^2-y^2}$ orbitals and in the region $1/2 < x < 1$ holes are doped into the d_{z^2} orbitals [39,64]. Measurements of Hall coefficient for $\text{La}_{2-x}\text{Sr}_x\text{NiO}_4$ by T. Katsufuji *et al.* [65], revealed that the charge carriers change from electronlike to holelike while going from the hole density $x < 1/3$ to $x > 1/3$.

In the undoped La_2NiO_4 , the oxidation state of nickel is Ni^{2+} with the electronic configuration $[\text{Ar}]4s^03d^8$. Hence only d_{z^2} and $d_{x^2-y^2}$ orbitals are relevant in the doped compound $\text{La}_{2-x}\text{Sr}_x\text{NiO}_4$. The electron-phonon interaction term of the Hamiltonian is given by

$$H_{\text{ep}} = -\frac{g\omega_0}{4} \sum_{i,j} (d_{z^2;i,j}^\dagger d_{x^2-y^2;i,j}^\dagger) \times \begin{pmatrix} q_{x;i,j} + q_{y;i,j} + 4q_{z;i,j} & -\sqrt{3}q_{x;i,j} + \sqrt{3}q_{y;i,j} \\ -\sqrt{3}q_{x;i,j} + \sqrt{3}q_{y;i,j} & 3q_{x;i,j} + 3q_{y;i,j} \end{pmatrix} \times \begin{pmatrix} d_{z^2;i,j} \\ d_{x^2-y^2;i,j} \end{pmatrix}, \quad (24)$$

where the distortions $q_{x;i,j} \equiv (a_{x;i,j}^\dagger + a_{x;i,j}) - (a_{x;i-1,j}^\dagger + a_{x;i-1,j})$, $q_{y;i,j} \equiv (b_{y;i,j}^\dagger + b_{y;i,j}) - (b_{y;i,j-1}^\dagger + b_{y;i,j-1})$, and $q_{z;i,j} \equiv (c_{z;i,j}^\dagger + c_{z;i,j})$. In the undoped compound, since both d_{z^2} and $d_{x^2-y^2}$ orbitals are occupied, there are only breathing mode distortions ($4q_{x;i,j} + 4q_{y;i,j} + 4q_{z;i,j}$) and no active Jahn-Teller (JT) distortions. Now, when we introduce holes in the system (by doping with Sr such that $0 < x < 1/2$), the holes occupy the $d_{x^2-y^2}$ orbitals; this is because a site with a single electron in $d_{x^2-y^2}$ orbital will produce in-plane distortions ($3q_x + 3q_y$) which have a greater incompatibility with the breathing mode distortions ($4q_x + 4q_y + 4q_z$) on the adjacent sites and thus cost more energy than a singly occupied d_{z^2} orbital. These $d_{x^2-y^2}$ holes can hop and are responsible for the transport properties. Each site with a $d_{x^2-y^2}$ hole is JT active.

The Hamiltonian for cooperative Jahn-Teller (CJT) distortions in the two-dimensional LSNO system involves holes in $d_{x^2-y^2}$ orbitals as the active carriers. The starting Hamiltonian H_{LSNO} , describing $\text{La}_{2-x}\text{Sr}_x\text{NiO}_4$ for $0 \leq x \leq 0.5$, consists of the following terms expressed in terms of the creation (destruction) operator $h_{i,j}^\dagger$ ($h_{i,j}$) for the holes in $d_{x^2-y^2}$ orbitals: (i) hopping term:

$$H_t' = \frac{3t}{4} \sum_{i,j} (h_{i+1,j}^\dagger h_{i,j} + h_{i,j+1}^\dagger h_{i,j} + \text{H.c.}); \quad (25)$$

(ii) hole-phonon interaction term:

$$H_l' = \frac{3}{4} g\omega_0 \sum_{i,j} [(a_{x;i,j}^\dagger + a_{x;i,j})(n_{i,j}^h - n_{i+1,j}^h) + (b_{y;i,j}^\dagger + b_{y;i,j})(n_{i,j}^h - n_{i,j+1}^h)]; \quad (26)$$

and (iii) lattice term:

$$H_l' = \omega_0 \sum_{i,j} (a_{x;i,j}^\dagger a_{x;i,j} + b_{y;i,j}^\dagger b_{y;i,j}), \quad (27)$$

where $n_{i,j}^h \equiv h_{i,j}^\dagger h_{i,j}$.

The Lang-Firsov transformed Hamiltonian is given by $\tilde{H}_{\text{LSNO}} = \exp(S)H_{\text{LSNO}}\exp(-S)$ where S has the form

$$S = \frac{3}{4}g \sum_{i,j} [(a_{x;i,j}^\dagger - a_{x;i,j})(n_{i,j}^h - n_{i+1,j}^h) + (b_{y;i,j}^\dagger - b_{y;i,j})(n_{i,j}^h - n_{i,j+1}^h)]. \quad (28)$$

Setting $t' = -3t/4$ and $g' = -3g/4$, in the nonadiabatic regime ($|t'|/\omega_0 \leq 1$) and at strong coupling (i.e., large g'^2), the transformed Hamiltonian can be split into two terms: the unperturbed Hamiltonian and the perturbation term. These two terms are the same as the ones given by Eqs. (5) and (6), except that they are written in hole-operator language; both γ and η are set to zero value; and t and g are replaced by t' and g' , respectively. If the carriers are taken to be HCBs instead of fermionic holes, then after following the same second-order perturbative procedure as in Sec. II, we end up with an effective Hamiltonian that is exactly the same as that given by Eq. (18) with $\gamma = 0 = \eta$ and with t and g being replaced by t' and g' , respectively. It is important to note that the small parameter value is again given by $[\frac{t^2}{2(E_p + V_p)\omega_0}]^{\frac{1}{2}}$ and remains unaltered. Now, since we are dealing with fermionic holes and not HCBs, we get the following effective Hamiltonian:

$$\begin{aligned} H'_{\text{eff}} = & -(E_p + 2V_z) \sum_{i,j} n_{i,j}^h \\ & - t_1 \sum_{i,j} (h_{i+1,j}^\dagger h_{i,j} + h_{i,j+1}^\dagger h_{i,j} + \text{H.c.}) \\ & + V_1 \sum_{i,j} (n_{i,j}^h n_{i+1,j}^h + n_{i,j}^h n_{i,j+1}^h) \\ & - t_2 \sum_{i,j} (h_{i+1,j+1}^\dagger (1 - n_{i+1,j}^h - n_{i,j+1}^h) h_{i,j} \\ & + h_{i-1,j+1}^\dagger (1 - n_{i-1,j}^h - n_{i,j+1}^h) h_{i,j} + \text{H.c.}) \\ & + V_2 \sum_{i,j} (n_{i,j}^h n_{i+1,j+1}^h + n_{i,j}^h n_{i-1,j+1}^h) \\ & - t_3 \sum_{i,j} (h_{i+2,j}^\dagger (1 - 2n_{i+1,j}^h) h_{i,j} \\ & + h_{i,j+2}^\dagger (1 - 2n_{i,j+1}^h) h_{i,j} + \text{H.c.}) \\ & + V_3 \sum_{i,j} (n_{i,j}^h n_{i+2,j}^h + n_{i,j}^h n_{i,j+2}^h), \quad (29) \end{aligned}$$

with $\gamma = 0 = \eta$ and with t and g being replaced by t' and g' , respectively. Since the interaction terms for the CJT Hamiltonian of LSNO are the same as those for the $t_1 - t_2 - t_3 - V_1 - V_2 - V_3$ Hamiltonian in Eq. (18), in LSNO also we expect to get the same charge-ordered phases obtained for the $t_1 - t_2 - t_3 - V_1 - V_2 - V_3$ model. Thus, at hole doping $1/2$ and $1/3$ (i.e., at $x = 1/2$ and $x = 1/3$ in $\text{La}_{2-x}\text{Sr}_x\text{NiO}_4$), we will realize checkerboard solid and diagonal stripes, respectively, which match exactly with the charge ordering obtained for LSNO experimentally.

Now, if we add one extra hole to the system at one-third hole doping (i.e., at $x = 1/3$), then the extra hole will reside in the region between two diagonal stripes. This extra hole can hop

anywhere in the region between the stripes without changing the potential energy of the system. Thus the carriers for the hole doping $x > 1/3$ are holes. On the other hand, adding one electron to the striped phase so that $x < 1/3$ will result in the extra electron occupying any one of the sites along the stripes; this extra electron is free to hop along the stripes without altering the potential energy of the system. This means that electrons are the carriers for the doping $x < 1/3$. Therefore, based on our model, we can explain the hole or electron doping (into the charge-ordered Mott insulator $\text{La}_{5/3}\text{Sr}_{1/3}\text{NiO}_4$) that was reported by T. Katsufuji *et al.* [65].

One can obviously ask how a system of HCBs can reproduce some experimental results of a system of electrons. The reason behind the charge orderings at hole-doping values $1/2$ and $1/3$ is repulsion; hopping does not play any role in the ordering. Hence, for these two CDWs, it does not matter whether the carriers of the system are HCBs or electrons. Close to one-third doping, only single carrier physics plays a role; consequently, particle-hole asymmetry is captured. Next, it is important to note that CJT interaction is needed to generate NNN and NNNN repulsions V_2 and V_3 which in turn are needed to explain diagonal stripes. Thus we see that our work resolves the controversy whether cooperative Jahn-Teller distortions can explain the observed diagonal-stripe charge order at one-third doping in LSNO [44–46]. Lastly, it should also be pointed out that, although experimentally [39] insulating behavior is observed in LSNO for $x \lesssim 0.9$, theoretically we expect metallic nature; we believe, this discrepancy is due to localization effects produced by disorder in real LSNO systems.

VI. CONCLUSIONS AND OPEN PROBLEMS

To conclude, we investigated a 2D system of HCBs, modulated by the cooperative breathing mode, which is important in real materials such as BaBiO_3 and nickelates as well as in artificial cold-atom systems. Using a duality treatment, we obtained the effective Hamiltonian and generated the phase diagram employing the SSE technique.

In the phase diagram displayed in Fig. 6, a first-order transition occurs from a superfluid to a checkerboard solid at filling-fraction $1/2$ and from a superfluid to a diagonal striped solid at filling $1/3$. We interpreted the nature of the transition by invoking Landau's explanation. It would be interesting to verify whether in other unfrustrated lattices, such as the checkerboard lattice, a discontinuous superfluid-solid transition is manifested at commensurate fillings such as $1/4$ [62]. Furthermore, at a fixed interaction strength, our $t_1 - t_2 - t_3 - V_1 - V_2 - V_3$ model realizes only continuous transitions (i.e., superfluid-supersolid and supersolid-solid transitions) as density is varied. Contrastingly, the $t_1 - t_2 - t_3 - V_1$ model (pertaining to the strong-coupling case of the Holstein model) manifests a discontinuous superfluid-supersolid transition when density is varied [21,22]. Thus, more insight is needed to identify which class of models yield what type of superfluid-supersolid transition.

We have identified the $t_1 - V_1 - V_2 - V_3$ model as the minimum model for obtaining a diagonal striped supersolid on a square lattice. It would be exciting to realize this system

in a cold-atom system, thereby adding to the understanding of lattice supersolidity generated by long-range interactions [13].

The asymmetry of the supersolid phase about a commensurate filling, such as one third in our case and one fourth in the case of Ref. [16], in a square lattice occurs possibly because particle-hole symmetry is not respected by the Hamiltonian about these fillings. It would be worthwhile to study the nature of such asymmetry in other lattices such as honeycomb, checkerboard, etc.

We have explained the charge ordering in $\text{La}_{2-x}\text{Sr}_x\text{NiO}_4$ at hole doping $x = 1/2$ and $1/3$ by considering cooperative Jahn-Teller effect. However, studies involving CJT effect are needed at dopings away from these fillings and particularly in the region $x > 1/2$ where holes are doped into the d_{z^2} orbitals. Also of interest would the explanation for the metal-insulator transition observed at $x \sim 0.9$ [39].

In a different but related system $\text{La}_{2-x}\text{Sr}_x\text{CoO}_4$, CDWs similar to those in LSNO are observed. At half-doping, there is a signature of checkerboard charge ordering with alternate Co^{2+} and Co^{3+} ions (below $T_{\text{CO}} \approx 750$ K) [66]. On the other hand, at the doping $x = 1/3$, the holes form a diagonal-stripe pattern similar to the stripes in LSNO at a transition temperature well above the room temperature [67–70]. Furthermore, the presence of substantial disorder in these diagonal stripes has been confirmed by the experiment [70] done by A. T. Boothroyd *et al.* The electronic configuration of cobalt is $[\text{Ar}]3d^74s^2$. In $\text{La}_{2-x}\text{Sr}_x\text{CoO}_4$, cobalt shows two different oxidation states: Co^{2+} and Co^{3+} . The Co^{3+} ions are found to have the low-spin ground state ($S = 0$) [71] with the electronic configuration $[\text{Ar}]3d^6$. In this case, all the six d electrons

occupy the t_{2g} orbitals and both the e_g orbitals are empty. Therefore Co^{3+} ions do not cause any Jahn-Teller distortion in the system. On the other hand, in the case of Co^{2+} ions, the electrons are in the high-spin ground state ($S = 3/2$) with the electronic configuration $[\text{Ar}]3d^7$. This state consists of five electrons in the t_{2g} orbitals and two in the e_g orbitals. Two out of the three t_{2g} orbitals are completely filled with four electrons, whereas the remaining orbital contains a single electron. Since both the e_g orbitals are occupied by one electron each, JT distortion comes into play due to the singly occupied t_{2g} orbital only. Owing to the fact that the JT distortion arising from t_{2g} electrons is weaker than the one arising from e_g electrons, it needs to be examined whether this can explain the disorder in the stripe pattern in $\text{La}_{2-x}\text{Sr}_x\text{CoO}_4$.

ACKNOWLEDGMENTS

The computing resources of the Condensed Matter Physics Division (Saha Institute of Nuclear Physics) have been used extensively. Valuable discussions with R. Pankaj are acknowledged. A.G. would especially like to thank S. Kar, G. Majumdar, and M. Sarkar for useful discussions regarding SSE. S.Y. thanks P. B. Littlewood for stimulating discussions and Cavendish laboratory for hospitality during the initial stages of this work.

APPENDIX A: NEAREST-NEIGHBOR REPULSION

The second-order perturbation term is given by

$$\begin{aligned}
 H^{(2)} &= - \sum_m \sum_{i,j,k,l} \frac{\langle 0 |_{\text{ph}} H_{1i,j} | m \rangle_{\text{ph}} \langle m |_{\text{ph}} H_{1k,l} | 0 \rangle_{\text{ph}}}{E_0^{\text{ph}} - E_m^{\text{ph}}} \\
 &= -t_1^2 \sum_m \sum_{i,j,k,l} \frac{1}{\Delta E_m^{\text{ph}}} \left[(d_{i+1,j}^\dagger d_{i,j} \langle 0 |_{\text{ph}} (\tau_{-x}^{ij} - 1) | m \rangle_{\text{ph}} + d_{i,j}^\dagger d_{i+1,j} \langle 0 |_{\text{ph}} (\tau_{+x}^{ij} - 1) | m \rangle_{\text{ph}} + d_{i,j+1}^\dagger d_{i,j} \langle 0 |_{\text{ph}} (\tau_{-y}^{ij} - 1) | m \rangle_{\text{ph}} \right. \\
 &\quad + d_{i,j}^\dagger d_{i,j+1} \langle 0 |_{\text{ph}} (\tau_{+y}^{ij} - 1) | m \rangle_{\text{ph}}) (d_{k+1,l}^\dagger d_{k,l} \langle m |_{\text{ph}} (\tau_{+x}^{kl} - 1) | 0 \rangle_{\text{ph}} + d_{k,l}^\dagger d_{k+1,l} \langle m |_{\text{ph}} (\tau_{-x}^{kl} - 1) | 0 \rangle_{\text{ph}} \\
 &\quad \left. + d_{k,l+1}^\dagger d_{k,l} \langle m |_{\text{ph}} (\tau_{+y}^{kl} - 1) | 0 \rangle_{\text{ph}} + d_{k,l}^\dagger d_{k,l+1} \langle m |_{\text{ph}} (\tau_{-y}^{kl} - 1) | 0 \rangle_{\text{ph}} \right], \tag{A1}
 \end{aligned}$$

where $t_1 = te^{-(E_p+V_p)/\omega_0}$ and $\Delta E_m^{\text{ph}} = E_0^{\text{ph}} - E_m^{\text{ph}}$.

As already mentioned in Sec. II A, the NN repulsion results from a process where a particle hops to its neighboring site and returns back, which in 2D consists of two terms: $\sum_{i,j} [n_{i,j}(1 - n_{i+1,j}) + n_{i+1,j}(1 - n_{i,j})]$ and $\sum_{i,j} [n_{i,j}(1 - n_{i,j+1}) + n_{i,j+1}(1 - n_{i,j})]$.

Since, $\sum_{i,j} n_{i,j}(1 - n_{i+1,j}) = \sum_{i,j} n_{i+1,j}(1 - n_{i,j})$ and $\sum_{i,j} n_{i,j}(1 - n_{i,j+1}) = \sum_{i,j} n_{i,j+1}(1 - n_{i,j})$, so the process is effectively given by $\sum_{i,j} [n_{i,j}(1 - n_{i+1,j}) + n_{i,j}(1 - n_{i,j+1})]$ with the coefficient doubled.

Now, we can rewrite the term $\sum_{i,j} n_{i,j}(1 - n_{i+1,j})$ as

$$\begin{aligned}
 \sum_{i,j} d_{i,j}^\dagger d_{i,j} (1 - d_{i+1,j}^\dagger d_{i+1,j}) &= \sum_{i,j} d_{i,j}^\dagger d_{i,j} d_{i+1,j} d_{i+1,j}^\dagger \\
 &= \sum_{i,j} d_{i,j}^\dagger d_{i+1,j} d_{i+1,j}^\dagger d_{i,j}.
 \end{aligned}$$

Looking at the expression of $H^{(2)}$, one can figure out that the above term comes from the multiplication of the terms $d_{i,j}^\dagger d_{i+1,j}$ and $d_{k+1,l}^\dagger d_{k,l}$ for $k = i$ and $l = j$. So, the coefficient of this term is given by

$$t_1^2 \sum_m \frac{\langle 0 |_{\text{ph}} (\tau_{+x}^{ij} - 1) | m \rangle_{\text{ph}} \langle m |_{\text{ph}} (\tau_{+x}^{ij} - 1) | 0 \rangle_{\text{ph}}}{\Delta E_m^{\text{ph}}}, \tag{A2}$$

where

$$\begin{aligned}
 \tau_{+x}^{ij} &= \exp[g(2a_{i,j} - a_{i-1,j} - a_{i+1,j}) + g(b_{i+1,j-1} \\
 &\quad + b_{i,j} - b_{i,j-1} - b_{i+1,j}) + \gamma g(c_{i,j} - c_{i+1,j})];
 \end{aligned}$$

consequently, the coefficient simplifies exactly to be $\frac{t_1^2}{\omega_0} G_9(4, 1, 1, 1, 1, 1, 1, \gamma^2, \gamma^2)$. Now, the general form

$G_n(\alpha_1, \alpha_2, \dots, \alpha_n)$ can be expressed as

$$G_n(\alpha_1, \alpha_2, \dots, \alpha_n) = \sum'_{m_1, m_2, \dots, m_n} \frac{(\alpha_1 g^2)^{m_1} \dots (\alpha_n g^2)^{m_n}}{m_1! \dots m_n! (m_1 + \dots + m_n)},$$

where $m_i = 0, 1, 2, \dots, \infty$ and the prime in \sum' implies the case $m_1 = m_2 = \dots = m_n = 0$ is excluded from the summation. It is important to note that for large values of g^2 , G_n can be approximately expressed as

$$G_n(\alpha_1, \alpha_2, \dots, \alpha_n) \approx \frac{\exp\left(\sum_{i=1}^n \alpha_i g^2\right)}{\sum_{i=1}^n \alpha_i g^2}. \quad (\text{A3})$$

Then, the NN repulsion is given by

$$-V_z \sum_{i,j} [n_{i,j}(1 - n_{i+1,j}) + n_{i,j}(1 - n_{i,j+1})], \quad (\text{A4})$$

where

$$\begin{aligned} V_z &= \frac{2t^2 e^{-2(E_p + V_p)/\omega_0}}{\omega_0} G_9(4, 1, 1, 1, 1, 1, 1, \gamma^2, \gamma^2) \\ &\approx \frac{2t^2}{2E_p + 2V_p}. \end{aligned} \quad (\text{A5})$$

Now, in arriving at Eq. (A4), we did not take into account the occupancy of the neighbors of the intermediate site. For example, when the particle hops from site (i, j) to NN site $(i + 1, j)$ and back, we have not considered the occupancy of the sites $(i + 2, j)$, $(i + 1, j + 1)$ and $(i + 1, j - 1)$, which are the neighboring sites of the intermediate site $(i + 1, j)$ (as can be seen from Fig. 1). We will consider this occupancy in the next appendix.

APPENDIX B: NNN REPULSION AND NNNN REPULSION

In this appendix, we first outline the procedure of calculating the coefficient of next-nearest-neighbor (NNN) repulsion, which occurs along the diagonals. Consider the case where a particle hops to its neighboring site and returns back yielding the term $\propto \sum_{\langle i,j \rangle} n_i(1 - n_j)$ with $\langle i, j \rangle$ indicating nearest-neighbor (NN) pairs of sites. In this process, we have to take into account the occupancy of the neighboring sites of the intermediate site j . For example, in Fig. 12, if a particle at site 1 hops to site 2 and comes back, then the coefficient of this process depends on the occupancy of the sites 3, 4, and 5. If all the three sites are empty, then this term can be expressed as $-V_z n_1(1 - n_3)(1 - n_4)(1 - n_5)$, where $V_z \approx \frac{2t^2}{2E_p + 2V_p}$; here, we have omitted the term $(1 - n_2)$ because the possibility of NN occupancy (for particle at site 1) is already excluded from the process due to the large value of NN repulsion $2V_p$. Due to numerical difficulties in our simulations using SSE, we need to simplify the four-operator term into a two-operator one by applying mean field to the remaining two operators. One can easily see that this mean-field procedure leaves us with a term which represents NNN repulsion (which acts along the diagonals) or NNNN repulsion (which acts along the axes).

We will now calculate the NNN repulsion coefficient which pertains to the diagonals of the square lattice in Fig. 12. To this end, we consider all the possible processes yielding the operator $n_1 n_3$ and add all the corresponding

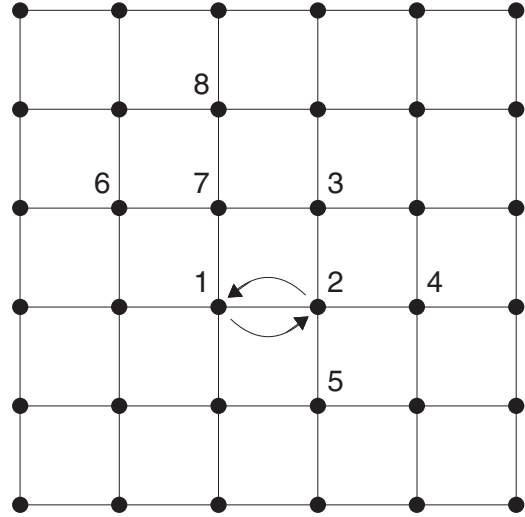


FIG. 12. Pictorial description of the process where a particle at site 1 hops to site 2 and comes back.

terms to evaluate its coefficient. The following are the relevant cases.

Case 1. NNN interaction, when all the three neighboring sites of the intermediate site are unoccupied, involves the following. (i) The contribution of particle hopping from site 1 to site 2 and coming back can be written as

$$\begin{aligned} & -\frac{2t^2}{(2E_p + 2V_p)} n_1(1 - n_3)(1 - n_4)(1 - n_5) \\ & \approx -\frac{2t^2}{(2E_p + 2V_p)} n_1(1 - n_3)\langle 1 - n_4 \rangle \langle 1 - n_5 \rangle \\ & \approx -\frac{2t^2}{(2E_p + 2V_p)} n_1(1 - n_3) \left(\frac{1}{2} - m\right)^2, \end{aligned} \quad (\text{B1})$$

where $\langle \dots \rangle$ implies mean value and $\langle 1 - n_4 \rangle = \langle 1 - n_5 \rangle = \left(\frac{1}{2} - m\right)$ with m being the magnetization of the system. (ii) The contribution of particle hopping from site 1 to site 7 and returning back involves a similar situation as (i) and is given as

$$\begin{aligned} & \approx -\frac{2t^2}{(2E_p + 2V_p)} n_1(1 - n_3)\langle 1 - n_6 \rangle \langle 1 - n_8 \rangle \\ & \approx -\frac{2t^2}{(2E_p + 2V_p)} n_1(1 - n_3) \left(\frac{1}{2} - m\right)^2. \end{aligned} \quad (\text{B2})$$

(iii) The contribution of particle hopping from site 3 to site 2 and coming back:

$$\begin{aligned} & \approx -\frac{2t^2}{(2E_p + 2V_p)} n_3(1 - n_1)\langle 1 - n_4 \rangle \langle 1 - n_5 \rangle \\ & \approx -\frac{2t^2}{(2E_p + 2V_p)} n_3(1 - n_1) \left(\frac{1}{2} - m\right)^2. \end{aligned} \quad (\text{B3})$$

(iv) The particle hopping from site 3 to site 7 and returning back is similar to (iii) and yields the same expression as Eq. (B3).
(v) The contribution of particle hopping from site 4 to site 2

and coming back:

$$\begin{aligned} &\approx -\frac{2t^2}{(2E_p + 2V_p)}(1 - n_3)(1 - n_1)\langle n_4 \rangle(1 - n_5) \\ &\approx -\frac{2t^2}{(2E_p + 2V_p)}(1 - n_3)(1 - n_1)\left(\frac{1}{4} - m^2\right)^2. \end{aligned} \quad (\text{B4})$$

(vi) The contribution of particle hopping from site 5 to site 2 and coming back is similar to (v) and is given by Eq. (B4). (vii) The particle hopping from site 6 to site 7 and returning back is also similar to (v) and the contribution is again given by Eq. (B4). (viii) The contribution of particle hopping from site 8 to site 7 and coming back is also similar to (v) and hence is given by Eq. (B4). Adding all the contributions for case 1, we get the coefficient of $n_1 n_3$ to be

$$\frac{2t^2}{(2E_p + 2V_p)}\left[4\left(\frac{1}{2} - m\right)^2 - 4\left(\frac{1}{4} - m^2\right)\right]. \quad (\text{B5})$$

Case 2. We consider contribution to NNN interaction when, among the three sites that are NN to the intermediate site, one of them is occupied and the other two are empty. Thus, compared to case 1, there is an extra repulsion term $2V_p$ in the denominator of the coefficient. Then, NNN interaction involves the following. (i) The particle hops from site 1 to site 2 and comes back. Any one of the three neighboring sites of site 2, i.e., 3, 4, or 5, is occupied; then, the contribution is

$$\begin{aligned} &\approx -\frac{2t^2}{(2E_p + 4V_p)}[n_1 n_3(1 - n_4)\langle 1 - n_5 \rangle \\ &\quad + n_1(1 - n_3)\langle n_4 \rangle(1 - n_5) + n_1(1 - n_3)(1 - n_4)\langle n_5 \rangle] \\ &\approx -\frac{2t^2}{(2E_p + 4V_p)}\left[n_1 n_3\left(\frac{1}{2} - m\right)^2\right. \\ &\quad \left.+ 2n_1(1 - n_3)\left(\frac{1}{4} - m^2\right)\right]. \end{aligned} \quad (\text{B6})$$

(ii) The particle hops from site 1 to site 7 and comes back. The situation is similar to (i) and hence the contribution is given by Eq. (B6). (iii) The particle hops from site 3 to site 2 and comes back. The resulting contribution is

$$\begin{aligned} &\approx -\frac{2t^2}{(2E_p + 4V_p)}[n_3 n_1(1 - n_4)\langle 1 - n_5 \rangle \\ &\quad + n_3(1 - n_1)\langle n_5 \rangle(1 - n_4) + n_3(1 - n_1)\langle n_4 \rangle(1 - n_5)] \\ &\approx -\frac{2t^2}{(2E_p + 4V_p)}\left[n_1 n_3\left(\frac{1}{2} - m\right)^2\right. \\ &\quad \left.+ 2n_3(1 - n_1)\left(\frac{1}{4} - m^2\right)\right]. \end{aligned} \quad (\text{B7})$$

(iv) The particle hops from site 3 to site 7 and returns back. Since the situation is similar to (iii), the contribution is expressed by Eq. (B7). (v) The particle hops from site 4 to site 2 and comes back. The contribution is

$$\begin{aligned} &\approx -\frac{2t^2}{(2E_p + 4V_p)}[\langle n_4 \rangle(1 - n_1)n_3(1 - n_5) \\ &\quad + \langle n_4 \rangle n_1(1 - n_3)(1 - n_5) + \langle n_4 \rangle(1 - n_1)(1 - n_3)\langle n_5 \rangle] \end{aligned}$$

$$\begin{aligned} &\approx -\frac{2t^2}{(2E_p + 4V_p)}\left[n_1(1 - n_3)\left(\frac{1}{4} - m^2\right)\right. \\ &\quad \left.+ n_3(1 - n_1)\left(\frac{1}{4} - m^2\right) + (1 - n_1)(1 - n_3)\left(\frac{1}{2} + m\right)^2\right]. \end{aligned} \quad (\text{B8})$$

(vi) The particle hops from site 5 to site 2 and comes back. The situation being similar to (v) leads to the contribution being given by Eq. (B8). (vii) The particle hops from site 6 to site 7 and comes back; this circumstance is also similar to (v) and hence contribution same as in Eq. (B8). (viii) The particle hops from site 8 to site 7 and comes back. Here too the contribution is given by Eq. (B8) since the circumstance is again similar to (v). Therefore, for case 2, the sum total of the above contributions yields the coefficient of $n_1 n_3$ to be

$$\frac{2t^2}{(2E_p + 4V_p)}\left[16\left(\frac{1}{4} - m^2\right) - 4\left(\frac{1}{2} - m\right)^2 - 4\left(\frac{1}{2} + m\right)^2\right]. \quad (\text{B9})$$

Case 3. Contribution to NNN interaction when the intermediate site has any two of the three NN sites occupied with the other being empty. Then, compared to case 2, the coefficient has an extra repulsion term $2V_p$ in the denominator; consequently, NNN interaction involves the following. (i) The particle hops from site 1 to site 2 and comes back; the resulting contribution is

$$\begin{aligned} &\approx -\frac{2t^2}{(2E_p + 6V_p)}[n_1 n_3 \langle n_4 \rangle(1 - n_5) \\ &\quad + n_1 n_3(1 - n_4)\langle n_5 \rangle + n_1(1 - n_3)\langle n_4 \rangle \langle n_5 \rangle] \\ &\approx -\frac{2t^2}{(2E_p + 6V_p)}\left[2n_1 n_3\left(\frac{1}{4} - m^2\right)\right. \\ &\quad \left.+ n_1(1 - n_3)\left(\frac{1}{2} + m\right)^2\right]. \end{aligned} \quad (\text{B10})$$

(ii) The particle hops from site 1 to site 7 and comes back. This situation is similar to (i) with the contribution being expressed by Eq. (B10). (iii) The particle hops from site 3 to site 2 and returns; the ensuing contribution is

$$\begin{aligned} &\approx -\frac{2t^2}{(2E_p + 6V_p)}[n_3 n_1(1 - n_4)\langle n_5 \rangle \\ &\quad + n_3 n_1 \langle n_4 \rangle(1 - n_5) + n_3(1 - n_1)\langle n_4 \rangle \langle n_5 \rangle] \\ &\approx -\frac{2t^2}{(2E_p + 6V_p)}\left[2n_1 n_3\left(\frac{1}{4} - m^2\right)\right. \\ &\quad \left.+ n_3(1 - n_1)\left(\frac{1}{2} + m\right)^2\right]. \end{aligned} \quad (\text{B11})$$

(iv) The particle hops from site 3 to site 7 and comes back. The situation is similar to (iii) with the contribution being given by Eq. (B11). (v) The particle hops from site 4 to site 2

and returns. This produces the contribution

$$\begin{aligned} &\approx -\frac{2t^2}{(2E_p + 6V_p)}[\langle n_4 \rangle n_1 n_3 \langle 1 - n_5 \rangle \\ &\quad + \langle n_4 \rangle (1 - n_1) n_3 \langle n_5 \rangle + \langle n_4 \rangle n_1 (1 - n_3) \langle n_5 \rangle] \\ &\approx -\frac{2t^2}{(2E_p + 6V_p)} \left[n_1 n_3 \left(\frac{1}{4} - m^2 \right) \right. \\ &\quad \left. + n_1 (1 - n_3) \left(\frac{1}{2} + m \right)^2 + n_3 (1 - n_1) \left(\frac{1}{2} + m \right)^2 \right]. \quad (\text{B12}) \end{aligned}$$

(vi) The particle hops from site 5 to site 2 and comes back. The circumstance, being similar to (v), yields the contribution expressed in Eq. (B12). (vii) The particle hops from site 6 to site 7 and comes back. The situation is also similar to (v) with the contribution being also given by Eq. (B12). (viii) The particle hops from site 8 to site 7 and returns. Again the situation is similar to (v) with the contribution being again given by Eq. (B12). Therefore, on adding all the various contributions for case 3, we get the coefficient of $n_1 n_3$ to be

$$\frac{2t^2}{(2E_p + 6V_p)} \left[12 \left(\frac{1}{2} + m \right)^2 - 12 \left(\frac{1}{4} - m^2 \right) \right]. \quad (\text{B13})$$

Case 4. Contribution to NNN interaction when all of the three neighboring sites of the intermediate site are occupied. Here, compared to case 3, the coefficient has an extra repulsion term $2V_p$ in the denominator. Then, NNN interaction involves the following. (i) The particle hops from site 1 to site 2 and comes back. Consequently, the contribution is

$$\begin{aligned} &\approx -\frac{2t^2}{(2E_p + 8V_p)} n_1 n_3 \langle n_4 \rangle \langle n_5 \rangle \\ &\approx -\frac{2t^2}{(2E_p + 8V_p)} n_1 n_3 \left(\frac{1}{2} + m \right)^2. \quad (\text{B14}) \end{aligned}$$

For all the following also the contribution is expressed by Eq. (B14) because the situation is similar to (i). (ii) The particle hops from site 1 to site 7 and comes back. (iii) The particle hops from site 3 to site 2 and returns. (iv) The particle hops from site 3 to site 7 and comes back. (v) The particle hops from site 4 to site 2 and comes back. (vi) The particle hops from site 5 to site 2 and returns. (vii) The particle hops from site 6 to site 7 and comes back. (viii) The particle hops from site 8 to site 7 and returns. Therefore, for case 4, the coefficient of $n_1 n_3$ is given by

$$-\frac{2t^2}{(2E_p + 8V_p)} \times 8 \left(\frac{1}{2} + m \right)^2. \quad (\text{B15})$$

Combining Eqs. (B5), (B9), (B13), and (B15), we finally get the coefficient of NNN repulsion (which acts along the diagonals) to be

$$\begin{aligned} V_2 = 2t^2 &\left[\left(\frac{1}{2} - m \right)^2 \frac{2V_p}{(E_p + V_p)(E_p + 2V_p)} \right. \\ &+ \left(\frac{1}{4} - m^2 \right) \frac{4E_p V_p}{(E_p + V_p)(E_p + 2V_p)(E_p + 3V_p)} \\ &\left. + \left(\frac{1}{2} + m \right)^2 \frac{2E_p V_p}{(E_p + 2V_p)(E_p + 3V_p)(E_p + 4V_p)} \right]. \quad (\text{B16}) \end{aligned}$$

To calculate the NNNN repulsion along the x axis (y axis), we have to consider all the processes from which a term $n_1 n_4$ ($n_1 n_8$) can appear. Adding all those terms, we can see that the coefficient of NNNN repulsion is just half of the coefficient of NNN repulsion. The reason for this is that the relevant contributions are from only half of the eight situations considered in each of the above four occupancy cases (i.e. the four cases involving different number of occupied neighbors for the intermediate site).

APPENDIX C: NNN HOPPING AND NNNN HOPPING

There are two possible hopping paths for a particle to arrive at a NNN site along the diagonals of the square lattice. For example, in Fig. 13, consider a particle hopping from site 1 to site 3. It can either hop to site 2 first and then to site 3 or it can hop to site 4 followed by a hop to site 3. Now, the coefficient of this process gets modified by the occupancy of the neighboring sites of the intermediate site. Without taking into account this effect, the process along any one path [on using Eq. (A1)] is given exactly by

$$-\frac{t^2 e^{-2(E_p + V_p)/\omega_0}}{\omega_0} G_5(2, 2, 1, 1, \gamma^2) \sum_{\langle\langle i, j \rangle\rangle} (d_i^\dagger d_j + \text{H.c.}),$$

where $\langle\langle i, j \rangle\rangle$ denotes NNN pairs of sites along the diagonals. For large values of g^2 , we have the following simplification for the coefficient in the above expression:

$$\frac{t^2 e^{-2(E_p + V_p)/\omega_0}}{\omega_0} G_5(2, 2, 1, 1, \gamma^2) \approx \frac{t^2 e^{-E_p/\omega_0}}{E_p + 2V_p}.$$

Path 1. The particle hops from site 1 to site 3 via site 2. The coefficient of this process depends on the occupancy of the sites 5 and 6, which are the two neighboring sites of the intermediate site 2.

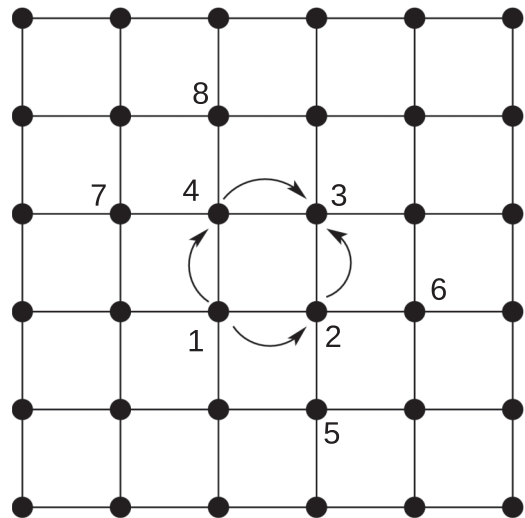


FIG. 13. Pictorial depiction of the process where a particle at site 1 hops to site 3, which is its NNN site along diagonal. The two possible paths for this process are indicated: hopping to site 3 via site 2 and site 4.

Case 1. Contribution to NNN hopping when both the neighboring sites are empty:

$$\begin{aligned} & -\frac{t^2 e^{-E_p/\omega_0}}{E_p + 2V_p} d_3^\dagger d_1 (1 - n_5)(1 - n_6) \\ & \approx -\frac{t^2 e^{-E_p/\omega_0}}{E_p + 2V_p} d_3^\dagger d_1 \langle 1 - n_5 \rangle \langle 1 - n_6 \rangle \\ & \approx -\frac{t^2 e^{-E_p/\omega_0}}{E_p + 2V_p} \left(\frac{1}{2} - m\right)^2 d_3^\dagger d_1. \end{aligned} \quad (\text{C1})$$

Case 2. Contribution when any one of the neighboring sites is occupied (giving an extra repulsion $2V_p$ in the denominator) and the other site is empty:

$$\begin{aligned} & \approx -\frac{t^2 e^{-E_p/\omega_0}}{E_p + 4V_p} d_3^\dagger d_1 [\langle n_5 \rangle \langle 1 - n_6 \rangle + \langle 1 - n_5 \rangle \langle n_6 \rangle] \\ & \approx -\frac{2t^2 e^{-E_p/\omega_0}}{E_p + 4V_p} \left(\frac{1}{4} - m^2\right) d_3^\dagger d_1. \end{aligned} \quad (\text{C2})$$

Case 3. Contribution when both the NN sites are occupied:

$$\begin{aligned} & \approx -\frac{t^2 e^{-E_p/\omega_0}}{E_p + 6V_p} d_3^\dagger d_1 \langle n_5 \rangle \langle n_6 \rangle \\ & \approx -\frac{t^2 e^{-E_p/\omega_0}}{E_p + 6V_p} \left(\frac{1}{2} + m\right)^2 d_3^\dagger d_1. \end{aligned} \quad (\text{C3})$$

Therefore, for path 1, we get the coefficient of $d_3^\dagger d_1$ to be

$$\begin{aligned} & -t^2 e^{-E_p/\omega_0} \left[\left(\frac{1}{2} - m\right)^2 \frac{1}{E_p + 2V_p} + \left(\frac{1}{4} - m^2\right) \frac{2}{E_p + 4V_p} \right. \\ & \left. + \left(\frac{1}{2} + m\right)^2 \frac{1}{E_p + 6V_p} \right]. \end{aligned} \quad (\text{C4})$$

Path 2. The particle hops from site 1 to site 4 first and then to site 3. The coefficient of this process gets modified depending on whether the sites 7 and 8 (NN to the intermediate site 4) are occupied or not.

Case 1. Contribution when both the neighboring sites are empty. This situation is similar to case 1 of path 1; hence the contribution is given by Eq. (C1).

Case 2. Contribution when any one of the neighboring sites is occupied and the other one is empty. This is similar to

case 2 of path 1; consequently, the contribution is expressed by Eq. (C2).

Case 3. Contribution when both the NN sites are occupied. This circumstance is similar to case 3 of path 1; thus, the contribution is given by Eq. (C3).

Thus we see that path 2 yields the same coefficient [given by Eq. (C4)] for $d_3^\dagger d_1$ as path 1. Combining the contributions from both the paths, a particle hopping to its NNN along diagonals can be expressed as $-t_2 \sum_{\langle\langle i,j \rangle\rangle} (d_i^\dagger d_j + \text{H.c.})$, where the coefficient t_2 is given by

$$\begin{aligned} t_2 = & 2t^2 e^{-E_p/\omega_0} \left[\left(\frac{1}{2} - m\right)^2 \frac{1}{E_p + 2V_p} \right. \\ & \left. + \left(\frac{1}{4} - m^2\right) \frac{2}{E_p + 4V_p} + \left(\frac{1}{2} + m\right)^2 \frac{1}{E_p + 6V_p} \right]. \end{aligned} \quad (\text{C5})$$

For the case of NNNN hopping (which occurs along the axes), there is only one possible path. Hence, the relevant coefficient t_3 for NNNN hopping is half of the coefficient for NNN hopping, i.e., $t_3 = \frac{t_2}{2}$.

APPENDIX D: SSE BOND HAMILTONIAN

Our effective Hamiltonian for HCBs, written in units of $2t_1$, can be expressed in terms of bond operators as follows:

$$H = - \sum_{i=1}^3 \sum_{B_i} H_{B_i}, \quad (\text{D1})$$

where B_1 , B_2 , and B_3 represent NN, NNN, and NNNN bonds in our system, respectively. In the above expression H_{B_i} can further be written as a sum of diagonal (H_{1,B_i}) and off-diagonal (H_{2,B_i}) parts, i.e., $H_{B_i} = H_{1,B_i} + H_{2,B_i}$. The expressions for the diagonal and off-diagonal parts are given as

$$\begin{aligned} H_{1,B_i} & = C_i - \Delta_i S_{j(B_i)}^z S_{k(B_i)}^z + h_B (S_{j(B_i)}^z + S_{k(B_i)}^z), \\ H_{2,B_i} & = \frac{J_i}{2} (S_{j(B_i)}^+ S_{k(B_i)}^- + \text{H.c.}), \end{aligned} \quad (\text{D2})$$

where $J_1 = 1$, $C_i \equiv \Delta_i/4 + h_B + \epsilon_i$, $\epsilon_i \geq 0$, and $h_B = h/Z$; the coordination number $Z = 12$ for our problem. Furthermore, $j(B_i)$ and $k(B_i)$ refer to sites connecting the bond B_i . The parameter ϵ_i is introduced to ensure that the two-spin matrix elements always stay positive.

[1] M. Boninsegni and N. V. Prokof'ev, *Rev. Mod. Phys.* **84**, 759 (2012).
 [2] G. Bilbro and W. L. McMillan, *Phys. Rev. B* **14**, 1887 (1976).
 [3] A. M. Gabovich, A. I. Voitenko, and M. Ausloos, *Phys. Rep.* **367**, 583 (2002).
 [4] S. H. Blanton, R. T. Collins, K. H. Kelleher, L. D. Rotter, Z. Schlesinger, D. G. Hinks, and Y. Zheng, *Phys. Rev. B* **47**, 996 (1993).
 [5] R. L. Withers and J. A. Wilson, *J. Phys. C* **19**, 4809 (1986).

[6] J. Merino and R. H. McKenzie, *Phys. Rev. Lett.* **87**, 237002 (2001).
 [7] W. W. Fuller, P. M. Chaikin, and N. P. Ong, *Phys. Rev. B* **24**, 1333 (1981).
 [8] A. Rusydi, W. Ku, B. Schulz, R. Rauer, I. Mahns, D. Qi, X. Gao, A. T. S. Wee, P. Abbamonte, H. Eisaki, Y. Fujimaki, S. Uchida, and M. Rübhausen, *Phys. Rev. Lett.* **105**, 026402 (2010).
 [9] P. Abbamonte, G. Blumberg, A. Rusydi, A. Gozar, P. G. Evans, T. Siegrist, L. Venema, H. Eisaki, E. D. Isaacs, and G. A. Sawatzky, *Nature (London)* **431**, 1078 (2004).

- [10] A. Taraphder, R. Pandit, H. R. Krishnamurthy, and T. V. Ramakrishnan, *Int. J. Mod. Phys. B* **10**, 863 (1996).
- [11] For coexistence of superconductivity and antiferromagnetism in systems with strong electron-phonon interaction, see A. Y. Ganin, Y. Takabayashi, P. Jeglič, Denis Arčon, A. Potočnik, P. J. Baker, Y. Ohishi, M. T. McDonald, M. D. Tzirakis, A. McLennan, G. R. Darling, M. Takata, M. J. Rosseinsky, and K. Prassides, *Nature (London)* **466**, 221 (2010); M. Capone, M. Fabrizio, C. Castellani, and E. Tosatti, *Rev. Mod. Phys.* **81**, 943 (2009); O. Gunnarsson, *ibid.* **69**, 575 (1997).
- [12] C. M. Varma, *Phys. Rev. Lett.* **61**, 2713 (1988).
- [13] R. Landig, L. Hruby, N. Dogra, M. Landini, R. Mottl, T. Donner, and T. Esslinger, *Nature (London)* **532**, 476 (2016).
- [14] G. G. Batrouni and R. T. Scalettar, *Phys. Rev. Lett.* **84**, 1599 (2000).
- [15] F. Hébert, G. G. Batrouni, R. T. Scalettar, G. Schmid, M. Troyer, and A. Dorneich, *Phys. Rev. B* **65**, 014513 (2001).
- [16] L. Dang, M. Boninsegni, and L. Pollet, *Phys. Rev. B* **78**, 132512 (2008).
- [17] B. Capogrosso-Sansone, C. Trefzger, M. Lewenstein, P. Zoller, and G. Pupillo, *Phys. Rev. Lett.* **104**, 125301 (2010).
- [18] Y.-C. Chen, R. G. Melko, S. Wessel, and Y.-J. Kao, *Phys. Rev. B* **77**, 014524 (2008).
- [19] P. Sengupta, L. P. Pryadko, F. Alet, M. Troyer, and G. Schmid, *Phys. Rev. Lett.* **94**, 207202 (2005).
- [20] G. Schmid and M. Troyer, *Phys. Rev. Lett.* **93**, 067003 (2004).
- [21] S. Kar and S. Yarlagadda, *Ann. Phys.* **375**, 322 (2016).
- [22] S. Datta and S. Yarlagadda, *Solid State Commun.* **150**, 2040 (2010).
- [23] X. Huo, Y.-Y. Cui, Dali Wang, and J.-P. Lv, *Phys. Rev. A* **95**, 023613 (2017).
- [24] S. Wessel and M. Troyer, *Phys. Rev. Lett.* **95**, 127205 (2005).
- [25] D. Heidarian and K. Damle, *Phys. Rev. Lett.* **95**, 127206 (2005).
- [26] A. Sen, P. Dutt, K. Damle, and R. Moessner, *Phys. Rev. Lett.* **100**, 147204 (2008).
- [27] R. G. Melko, A. Paramekanti, A. A. Burkov, A. Vishwanath, D. N. Sheng, and L. Balents, *Phys. Rev. Lett.* **95**, 127207 (2005).
- [28] M. Boninsegni and N. Prokof'ev, *Phys. Rev. Lett.* **95**, 237204 (2005).
- [29] R. G. Melko, A. Del Maestro, and A. A. Burkov, *Phys. Rev. B* **74**, 214517 (2006).
- [30] L. Pollet, J. D. Picon, H. P. Büchler, and M. Troyer, *Phys. Rev. Lett.* **104**, 125302 (2010).
- [31] S. Wessel, *Phys. Rev. B* **75**, 174301 (2007).
- [32] J. Y. Gan, Y. C. Wen, J. Ye, T. Li, S.-J. Yang, and Y. Yu, *Phys. Rev. B* **75**, 214509 (2007).
- [33] T. Mishra, R. V. Pai, and S. Mukerjee, *Phys. Rev. A* **89**, 013615 (2014).
- [34] A. Ghosh and S. Yarlagadda, *Phys. Rev. B* **90**, 045140 (2014).
- [35] T. Bilitewski and N. R. Cooper, *Phys. Rev. A* **94**, 023630 (2016).
- [36] For a review, see H. Ulbrich and M. Braden, *Physica C (Amsterdam)* **481**, 31 (2012).
- [37] C. H. Chen, S.-W. Cheong, and A. S. Cooper, *Phys. Rev. Lett.* **71**, 2461 (1993).
- [38] S.-W. Cheong, H. Y. Hwang, C. H. Chen, B. Batlogg, L. W. Rupp, Jr., and S. A. Carter, *Phys. Rev. B* **49**, 7088(R) (1994).
- [39] K. Ishizaka, Y. Taguchi, R. Kajimoto, H. Yoshizawa, and Y. Tokura, *Phys. Rev. B* **67**, 184418 (2003).
- [40] R. Kajimoto, T. Kakeshita, H. Yoshizawa, T. Tanabe, T. Katsufuji, and Y. Tokura, *Phys. Rev. B* **64**, 144432 (2001).
- [41] H. Yoshizawa, T. Kakeshita, R. Kajimoto, T. Tanabe, T. Katsufuji, and Y. Tokura, *Phys. Rev. B* **61**, R854(R) (2000).
- [42] P. G. Freeman, A. T. Boothroyd, D. Prabhakaran, M. Enderle, and C. Niedermayer, *Phys. Rev. B* **70**, 024413 (2004).
- [43] L. Rademaker, Y. Pramudya, J. Zaanen, and V. Dobrosavljević, *Phys. Rev. E* **88**, 032121 (2013).
- [44] T. Hotta and E. Dagotto, *Phys. Rev. Lett.* **92**, 227201 (2004).
- [45] S. Yamamoto, T. Fujiwara, and Y. Hatsugai, *Phys. Rev. B* **76**, 165114 (2007).
- [46] K. Rościszewski and A. M. Oleś, *J. Phys.: Condens. Matter* **23**, 265601 (2011).
- [47] A. Ghosh and S. Yarlagadda (unpublished).
- [48] In one dimension, it has been shown in Ref. [34] that $t_2 - V_1$ model yields a cSS. In 2D, it has been demonstrated in Ref. [21] that $t_2 - t_3 - V_1$ model generates a cSS; using similar logic, it can be shown that $t_2 - V_1$ model also manifests cSS.
- [49] P. B. Allen and V. Perebeinos, *Phys. Rev. B* **60**, 10747 (1999).
- [50] I. G. Lang and Yu. A. Firsov, *Zh. Eksp. Teor. Fiz.* **43**, 1843 (1962) [*Sov. Phys. JETP* **16**, 1301 (1963)].
- [51] R. Pankaj and S. Yarlagadda, *Phys. Rev. B* **86**, 035453 (2012).
- [52] S. Reja, S. Yarlagadda, and P. B. Littlewood, *Phys. Rev. B* **84**, 085127 (2011).
- [53] S. Reja, S. Yarlagadda, and P. B. Littlewood, *Phys. Rev. B* **86**, 045110 (2012).
- [54] A. Dey, M. Q. Lone, and S. Yarlagadda, *Phys. Rev. B* **92**, 094302 (2015).
- [55] A. W. Sandvik, *Phys. Rev. B* **56**, 11678 (1997).
- [56] A. W. Sandvik, *AIP Conf. Proc.* **1297**, 135 (2010).
- [57] O. F. Syljuåsen and A. W. Sandvik, *Phys. Rev. E* **66**, 046701 (2002).
- [58] O. F. Syljuåsen, *Phys. Rev. E* **67**, 046701 (2003).
- [59] G. G. Batrouni, R. T. Scalettar, G. T. Zimanyi, and A. P. Kampf, *Phys. Rev. Lett.* **74**, 2527 (1995).
- [60] O. Nguyen and L. Dang, *Eur. Phys. J. B* **90**, 71 (2017).
- [61] A. Kuklov, N. Prokofev, and B. Svistunov, *Phys. Rev. Lett.* **93**, 230402 (2004).
- [62] S. Wessel, *Phys. Rev. B* **86**, 140501(R) (2012).
- [63] The nature of the special points (i.e., whether they represent triple points, etc.) needs further investigation.
- [64] R. J. Cava, B. Batlogg, T. T. Palstra, J. J. Krajewski, W. F. Peck, Jr., A. P. Ramirez, and L. W. Rupp, Jr., *Phys. Rev. B* **43**, 1229(R) (1991).
- [65] T. Katsufuji, T. Tanabe, T. Ishikawa, S. Yamanouchi, Y. Tokura, T. Kakeshita, R. Kajimoto, and H. Yoshizawa, *Phys. Rev. B* **60**, R5097(R) (1999).
- [66] I. A. Zaliznyak, J. P. Hill, J. M. Tranquada, R. Erwin, and Y. Moritomo, *Phys. Rev. Lett.* **85**, 4353 (2000).
- [67] M. Cwik, M. Benomar, T. Finger, Y. Sidis, D. Senff, M. Reuther, T. Lorenz, and M. Braden, *Phys. Rev. Lett.* **102**, 057201 (2009).
- [68] A. T. Boothroyd, P. Babkevich, D. Prabhakaran, and P. G. Freeman, *Nature (London)* **471**, 341 (2011).
- [69] E. C. Andrade and M. Vojta, *Phys. Rev. Lett.* **109**, 147201 (2012).
- [70] T. Lancaster, S. R. Giblin, G. Allodi, S. Bordignon, M. Mazzani, R. De Renzi, P. G. Freeman, P. J. Baker, F. L. Pratt, P. Babkevich, S. J. Blundell, A. T. Boothroyd, J. S. Möller, and D. Prabhakaran, *Phys. Rev. B* **89**, 020405(R) (2014).
- [71] N. Hollmann, M. W. Haverkort, M. Cwik, M. Benomar, M. Reuther, A. Tanaka, and T. Lorenz, *New J. Phys.* **10**, 023018 (2008).